



**A WIGNER DISTRIBUTION ANALYSIS
OF ONE DIMENSIONAL SCATTERING**

THESIS

Brent R. Lacy, Captain, USAF

AFIT/GAP/ENP/09-M06

**DEPARTMENT OF THE AIR FORCE
AIR UNIVERSITY**

AIR FORCE INSTITUTE OF TECHNOLOGY

Wright-Patterson Air Force Base, Ohio

APPROVED FOR PUBLIC RELEASE; DISTRIBUTION UNLIMITED

The views expressed in this thesis are those of the author and do not reflect the official policy or position of the United States Air Force, Department of Defense, or the United States Government.

AFIT/GAP/ENP/09-M06

A WIGNER DISTRIBUTION ANALYSIS
OF ONE DIMENSIONAL SCATTERING

THESIS

Presented to the Faculty
Department of System and Engineering Management
Graduate School of Engineering and Management
Air Force Institute of Technology
Air University
Air Education and Training Command
In Partial Fulfillment of the Requirements for the
Degree of Master of Science in Applied Physics

Brent R. Lacy, BS

Captain, USAF

March 2009

APPROVED FOR PUBLIC RELEASE; DISTRIBUTION UNLIMITED

AFIT/GAP/ENP/09-M06

A WIGNER DISTRIBUTION ANALYSIS
OF ONE DIMENSIONAL SCATTERING

Brent R. Lacy, BS

Captain, USAF

Approved:



David E. Weeks (Chairman)

23 Mar 09
Date



William F. Bailey (Member)

20 Mar 2009
Date



Kevin C. Gross (Member)

19-Mar-09
Date

Abstract

We applied the Wigner Distribution Function, a distribution function of time and frequency based on an initial function of either of those variables, to a series of time based correlation functions. These time based correlation functions were the result of a 1-dimensional free particle wave packet, the reactant wave function, which had propagated through a quantum potential well and then had components of the reactant wave function that exited the opposite side of the well auto-correlated in time with a stationary 1-dimensional free particle wave packet, the product wave function. This process was undertaken in order to generate a 3-dimensional depiction, in time and frequency, of the reactant wave functions interaction with the quantum potential well. Fortran 77 code was utilized to generate the time propagation of the reactant wave function by means of the Split Operator Method, which was given the following initial set of conditions; $x_0 = -20$ (Bohr radii), $k_0 = 3$ (atomic units), and $\delta = 1$ (Bohr radius). A series of potential wells with variable depths were implemented into the code. The code then computed the correlation in time of the exiting reactant wave function with a stationary wave function before applying the Wigner Distribution Function. When Wigner Distribution Function was applied to the time correlation function many recognizable features on the potential well were observed from the 3-dimensional plot generated including transmission resonance energy levels. The classical time of arrival was also captured by the Wigner Distribution Function. As a useful tool the Wigner Distribution Function provides more insight into the quantum interactions of chemical reactions in terms of time and frequency than traditional spectrographic analysis.

Dedication

I would like to dedicate this work to my wife whose sheer love of me gave her the strength to endure the heights of insanity I reached during this research. Without her I'd be truly lost.

Acknowledgement

I would like to tip my hat to the pantheon of teachers and professor who have led me to this point, but most specifically to Professor Weeks, my advisor. Without your mentorship, knowledge, and abundance of patience with me I doubt this work would have come to completion. I feel I shall be in debt to you for an amount I can never truly repay.

Table of Contents

	Page
Abstract	iv
Dedication	v
Acknowledgement.....	vi
Table of Contents	vii
List of Figures	ix
List of Table	xiii
I. Introduction.....	1
1.1. Motivation	1
1.2. Problem Statement	5
1.3. Approach	5
II. Background.....	10
2.1. Fourier Transform	10
2.2. Wigner Distribution Function	11
2.3. Propagating Wave packet.....	13
2.4. Split Operator Method.....	17
2.5. Square Well Scattering.....	19
2.6. Time Correlation Function	23
2.7. Atomic Units	24
III. Numerical Approach	26
3.3. Fast Fourier Transform.....	26
3.4. Aliasing	27
3.5. Absorbing Boundaries.....	29
3.6. Free Particle Propagation	31
3.7. Coherent State of a Harmonic Oscillator.....	32
3.8. Discrete Wigner Distribution (DWD) Function	35
3.9. Down Sampling.....	36
IV. Results	38
4.1 Correlation Function.....	38
4.2 Wigner Distribution Plots.....	39
V. Analysis	46
5.1. Transmission Coefficients	46
5.2. Square Well Energy Levels	49
5.3. Time Arrivals	51
5.4. Spectrogram versus WDF	55
5.5. Conclusion.....	59
5.6. Further Research.....	60

	Page
Appendix A	61
Gaussian Well	62
Triangular Well	64
Appendix B	66
Appendix C	68
Bibliography.....	70
Vita.....	72

List of Figures

Figure	Page
1. The WDF of the initial wave function, $\psi(x, 0)$, of a free particle with an initial position of 0, an initial momentum of 1, and an initial spread of 1. We can see the overall Gaussian feature displayed in phase space shifted off center from the origin in the momentum axes. This is due to the wave function having an initial momentum of 1 which aligns with where the peak of the Gaussian is located in phase space with respect to the momentum axis.....	4
2. The initial setup of the reactant wave function and the product wave function positioned opposite each other from a square well. In this depiction the wave functions are simple Gaussian curves centered about 4 (dashed curve) and -4 (dotted curve) with a square well between them centered about the origin (solid line). The Gaussian to the left of the potential well is the reactant wave function and the Gaussian to the right of the potential well is the product wave function.....	6
3. The comparison of the probability distribution in both position and momentum of free particle wave function at $\psi(x, 0)$. The solid red lines represents the solution derived by taking the modulus of the wave function and the blue dots represent the solution of the integrate projection of the WDF with the axes of interest.	9
4. The time evolution of the real and imaginary components of a free particle with initial values of $x = -20$, $k = 3$, and a spread of 1.....	16
5. The transmission as a function of energy of a square well with depth, $V_o = 20$, and width, $2a = 20$	22
6. A propagating wave function incident on absorbing boundary potential.....	31
7. Comparison of the analytical form of a free particle wave function with the results of the split operator method. The blue dots represent the real part of the wave function as generated from the split operator method. The lines connecting the dots represent the analytical result of the real part of the wave function. The reason the wave function appears to leave the window and not cycle round again as discussed in this section is that the graphical depiction only shows a narrow portion (-20 to 50) of our x domain.	32
8. Comparison of the Coherent function ground state with the results from the split operator method. The blue dots represent the imaginary part of the wave function and the red dots represent the real part of the wave function as generated from the split operator method. The lines connecting the dots represent the analytical result and the colors are the converse for distinction between the lines and dots. In the analytical case the red line represents the imaginary part and the blue represents the real part.	34

Figure	Page
9. A correlation function, both its real and imaginary components, generated by the Fortran 77 code utilizing the Split Operator Method. Though only displayed from $t = 5$ to $t = 35$ the correlation function was captured for $t = 0.09$ to $t = 99.99$	38
10. The WDF of a free particles correlation function.....	40
11. Depiction of a WDF plot generated from the time correlation function of a reactant wave function scattering through a quantum potential well of $2E_h$. The red lines indicate frequencies of total transmission that correspond to a well of that depth.	42
12. Depiction of a WDF plot generated from the time correlation function of a reactant wave function scattering through a quantum potential well of $4E_h$. The red lines indicate frequencies of total transmission that correspond to a well of that depth.	42
13. Depiction of a WDF plot generated from the time correlation function of a reactant wave function scattering through a quantum potential well of $6E_h$. The red lines indicate frequencies of total transmission that correspond to a well of that depth.	42
14. Depiction of a WDF plot generated from the time correlation function of a reactant wave function scattering through a quantum potential well of $8E_h$. The red lines indicate frequencies of total transmission that correspond to a well of that depth.	42
15. Depiction of a WDF plot generated from the time correlation function of a reactant wave function scattering through a quantum square well of $10E_h$. The red lines indicate frequencies of total transmission that correspond to a well of that depth.	43
16. Depiction of a WDF plot generated from the time correlation function of a reactant wave function scattering through a quantum circular well of $10E_h$	43
17. Depiction of a WDF plot generated from the time correlation function of a reactant wave function scattering through a quantum square well of $20E_h$. The red lines indicate frequencies of total transmission that correspond to a well of that depth.	44
18. Depiction of a WDF plot generated from the time correlation function of a reactant wave function scattering through a quantum circular well of $20E_h$	44
19. Depiction of a WDF plot generated from the time correlation function of a reactant wave function scattering through a quantum square well of $40E_h$. The red lines indicate frequencies of total transmission that correspond to a well of that depth.	44
20. Depiction of a WDF plot generated from the time correlation function of a reactant wave function scattering through a quantum circular well of $40E_h$	44

Figure	Page
21. Depiction of a WDF plot generated from the time correlation function of a reactant wave function scattering through a quantum square well of $60E_h$. The red lines indicate frequencies of total transmission that correspond to a well of that depth.	45
22. Depiction of a WDF plot generated from the time correlation function of a reactant wave function scattering through a quantum circular well of $60E_h$	45
23. Depiction of a WDF plot generated from the time correlation function of a reactant wave function scattering through a quantum square well of $80E_h$. The red lines indicate frequencies of total transmission that correspond to a well of that depth.	45
24. Depiction of a WDF plot generated from the time correlation function of a reactant wave function scattering through a quantum circular well of $80E_h$	45
25. The integrated projection of the WDF in frequency is given by the blue dots and the transmission function of a square well of width $2a = 10$ and $V_o = 20$ is given by the solid blue line.	47
26. The comparison of the product of the transmission function (2.27) and equation (5.2) and the result of the integrated projection of the WDF upon the frequency axis. The red line is the product result and the blue dots are the results of the integration.....	48
27. WDF plot with total transmission energy level bands of a well width of $40E_h$. The red lines indicate allowed frequencies for a quantum square well of depth $40E_h$ and width of $20a_0$	50
28. WDF plot with total transmission energy level bands of a well width of $40E_h$. The red lines indicate allowed frequencies for a quantum square well of depth $40E_h$ and width of $40a_0$	51
29. A contour plot of the WDF with yellow lines indicating the arrival times of a classical particle with the given frequency/energy while the red line indicate allowed frequencies of the quantum well.	54
30. The windowed FT of our correlation function utilizing various FWHM values for the Gaussian window term. From right to left the value of c in equation (5.11) is as follows; 4.24661, 2.1233, 1.06165, 0.707768, and 0.530826 respectively.	56
31. A series of spectrogram plots of a correlation function of the scattering event involving a well of depth $40E_h$ and width of $20a_0$. The box indicates the size in comparison to the overall time domain that the Gaussian window function, equation (5.11), set to when the spectrogram was generated. A N^{th} window size corresponds to a Δt given by the overall time of the correlation function divided by N , $\Delta t/N = 99.99N$	57
32. The well shapes used as the potential component of the Spilt Operator Method. From right to left they are a square well, a circular well, a triangular well, and a Gaussian well.....	61

Figure	Page
33. Depiction of a WDF plot generated from the time correlation function of a reactant wave function scattering through a quantum Gaussian well of $10E_h$	62
34. Depiction of a WDF plot generated from the time correlation function of a reactant wave function scattering through a quantum Gaussian well of $20E_h$	62
35. Depiction of a WDF plot generated from the time correlation function of a reactant wave function scattering through a quantum Gaussian well of $40E_h$	63
36. Depiction of a WDF plot generated from the time correlation function of a reactant wave function scattering through a quantum Gaussian well of $60E_h$	63
37. Depiction of a WDF plot generated from the time correlation function of a reactant wave function scattering through a quantum Gaussian well of $80E_h$	64
38. Depiction of a WDF plot generated from the time correlation function of a reactant wave function scattering through a quantum triangular well of $10E_h$	65
39. Depiction of a WDF plot generated from the time correlation function of a reactant wave function scattering through a quantum triangular well of $20E_h$	65
40. Normalized spectrograms of the generated correlation function of the scattering event involving a well of depth $40E_h$ and width of $20a_0$. The red lines indicate the classical time arrival of a particle with energy given by ω and the yellow lines represent the allowed transmission resonances of the square well. Window sizes of a 10 th , 20 th , 30 th and 40 th of the overall time length of the correlation are given shown.....	66
41. Normalized spectrograms of the generated correlation function of the scattering event involving a well of depth $40E_h$ and width of $20a_0$. The red lines indicate the classical time arrival of a particle with energy given by ω and the yellow lines represent the allowed transmission resonances of the square well. Window sizes of a 50 th , 60 th , 70 th and 80 th of the overall time length of the correlation are given shown.....	67
42. Ambiguity function (real component on the left and imaginary component on the right) of a complex Gaussian centered about $x = 2.5$ and all other attributes set to unity.....	68
43. The modulus of a Ambiguity function of a complex Gaussian centered about $x = 2.5$ and all other attributes set to unity.....	69
44. The modulus of an Ambiguity Function of a correlation function generated from scattering through a quantum potential square well of depth $40E_h$ and width of $20a_0$. Represented on a logarithmic scale.	69

List of Table

Table	Page
1. Atomic Units System[12]	25
2. Comparison of grid sizes and grid step sizes for Discrete Fourier Transforms.....	29
3. Down sampling values	37

A WIGNER DISTRIBUTION ANALYSIS OF ONE DIMENSIONAL SCATTERING

I. Introduction

1.1. Motivation

In an overall sense, gaining an appreciation for how elements of a system change over time is the fundamental result of most scientific observation. In chemistry, one monitors the populations of reactant species and the resulting product species of compounds over the course of a chemical reaction. In physics, one observes the characteristics (mass, velocity, etc) of an element of a system and monitors how those characteristics change as the system evolves in time. Typically, these temporal observations are bookended observations of the reaction or interaction being monitored. That is to say, we generally observe things before the event in question and state the properties known of the system as the initial conditions. Once the event in question has occurred we again review the properties of the system and state that these are the outcomes. Development of techniques and procedures to aid in an effort to view and analysis the continuous evolution of a system would prove invaluable in the furtherance of scientific research.

Of immediate importance to the Air Force Office of Scientific Research is the development of tools and technique that would aid in the development and refinement of

Diode Pumped Alkaline Lasers (DPALs). In such a system, an Alkaline atom has had its electrons pumped into the $P_{3/2}$ state and then by means of scattering allowed to decay to the $P_{1/2}$ state. Due to the population inversion created between the $P_{1/2}$ state and the ground state, a situation for lasing is generated. Fully understanding how the scattering works in the decaying from the upper state to the lower one may aid in advancing techniques for making such Diode Pumped Lasers more efficient and feasible. As mentioned beforehand, the ability to monitor such interaction over time in a useful manner would be of great significance, but such techniques are difficult to apply due to the complexity of the interactions in question since they can occur in multiple dimensions and amongst several dependant variables.

One such way to monitor the development of a system in quantum mechanics and in physical chemistry is to develop a correlation function in time of two wave functions, one the reactant wave function and the other the product wave function. In this manner, the reactant wave function is allowed to react with the system in question over time while being correlated with a stationary product wave function which has no interaction with the system. This technique has many benefits as it records the information of the reactant wave function over time and eliminates the issues imposed by multidimensional or many valued problems as they reduce all the information of the system down to a scalar function of time, a signal. Once a signal of the interaction has been recorded, it is possible to apply many signal-processing techniques upon it to regain information about the initial interaction.

One such signal processing technique is the application of the Wigner Distribution Function (WDF). [1] In 1932, Eugene Wigner, in an attempt to return quantum mechanics to the domain of phase space, was able to generate a function of both position and momentum in phase space from the wave function in position space of a quantum state. This distribution¹ function's integrated projections onto either the position or momentum axes returned the probability densities of the wave equations for those variables respectively. The WDF is given by the form: [2]

$$W(x, p) = \frac{1}{\pi\hbar} \int \psi^*(x + y)\psi(x - y)e^{\frac{2ipy}{\hbar}} dy \quad (1-1)$$

where x is position, p is momentum, and ψ is the time independent wave function. This phase space picture of quantum mechanics is still very different from the classical phase space picture since the WDF can take on negative values and is a surface in a third axis rather than a parametric plot in the plane of the position and momentum. This feature predominantly arises from the Heisenberg Uncertainty Principle, which makes it impossible to simultaneously know both the position, and the simultaneous momentum, of a quantum mechanical system. Figure 1 shows a WDF of the initial wave function, $\psi(x, 0)$, of a free particle wave function with an initial position of 0, an initial momentum of 1, and an initial spread of 1^2 .

¹ This can easily be confused as meaning a probability distribution function, which the WDF is not due to the fact that it can take on negative values.

² The meaning behind these initial conditions and the equations that govern them will be illuminated in Section 2.3, but for completeness that are included here.

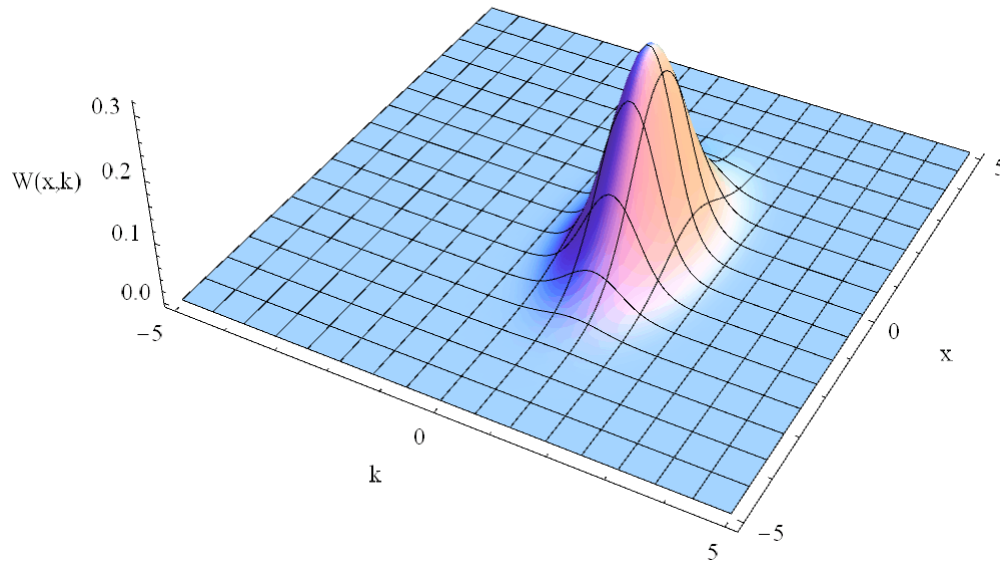


Figure 1. The WDF of the initial wave function, $\psi(x,0)$, of a free particle with an initial position of 0, an initial momentum of 1, and an initial spread of 1. We can see the overall Gaussian feature displayed in phase space shifted off center from the origin in the momentum axes. This is due to the wave function having an initial momentum of 1 which aligns with where the peak of the Gaussian is located in phase space with respect to the momentum axis

The WDF does not provide any new information than what was already determined by the individual wave equations. However, as much as a graph does not tell you anything more than the table of data it is representing, the WDF provides a new way of viewing the information obtained from the Schrödinger Equation. A similar relationship between time and frequency is present in all wave mechanics, as is displayed in position and momentum in quantum mechanics, so it is possible to extend the WDF to the time/frequency domain. Ultimately, the resulting depiction of the time and frequency

WDF could provide insightful representations of quantum mechanical events, such as the scattering of a wave packet upon potential wells and a means to characterize those events.

1.2. Problem Statement

We want to propagate a free particle reactant wave packet through a quantum potential well and compute its time correlation function with a stationary product wave packet. Then we want to apply a WDF to the time correlation function and analyze the results using known attributes of the quantum square well that the reactant wave packet had propagated through. Ultimately, we want to be able to compare these results with other signal processing techniques, such as a spectrogram of the same signal, and determine if the WDF is a viable or superior method of analyzing the time based signal results of a chemical or quantum reaction. Additionally, we want to determine whether the WDF gives us any further or new insight into the physics within the well past the initial scattering of the reactant wave function.

1.3. Approach

Solutions to the equations and procedures described in our problem will be difficult to achieve by analytical means alone. We will instead employ a wide variety of numerical techniques in order to simulate our wave packet scattering event in a computer model. By ensuring that we take sufficiently small numerical increments for each step, we will be able to provide the best approximation of the true analytical³ result.

³ By stating “true analytical result” it is tempting to believe I am referring to an actual analytical answer to our problem which is not the intent, but instead to highlight the analytical result that would have been obtained had it been possible to take the considerable amount of time necessary to mathematically construct a solution to the Hamiltonians being analyzed here. A process nature accomplished in considerably less time than men.

As the framework for our computer model we will define a set of position coordinates progressing from a defined $-x_{max}$ to x_{max} in increments of Δx . Using this x-grid we will discretely define a potential, $V(x)$, such that for all values within a and $-a$ of the origin the potential is a set negative value and zero for all other locations. This $V(x)$ will serve as our potential well. In this space we will position two wave packets on either side of the potential well ensuring that the wave functions are a sufficient distance from the well that the functional values will have sufficiently decreased to zero before occupying the same space as the well. The wave function to the left⁴ of the well will serve as the reactant wave function, $\Psi_R(x, 0)$, for our numerical wave function propagator, $\Psi_R(x, t)$, while the wave function to the right will serve as our product wave function, $\Psi_P(x, 0)$. Figure 2 depicts this initial setup.

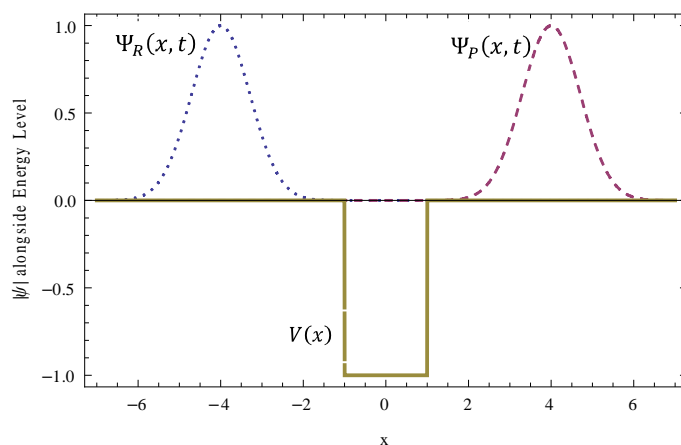


Figure 2. The initial setup of the reactant wave function and the product wave function positioned opposite each other from a square well. In this depiction the wave functions are simple Gaussian curves centered about 4 (dashed curve) and -4 (dotted curve) with a square well between them centered about the origin (solid line). The Gaussian to the left of the potential well is the reactant wave function and the Gaussian to the right of the potential well is the product wave function.

⁴ By left we mean the wave function is centered at a value of x less than the lower bound of the potential well. The inherent symmetry imposed by this setup is not an imposed restriction of our numerical method or has any specific benefit, but is purely a matter of preference and the methods applied could be applied to any 1 dimensional setup.

By taking the correlation of these two functions as time progress as the reactant wave function propagates towards the product wave function on the other side of the well, we will record the amplitude and frequency of the reactant wave function after it leaves its interaction with the well. This is possible since the product wave function is only known zero, within a numerically reasonable degree⁵, in the region just after the well in relationship to the reactant wave function so that when it is correlated it only has non-zero results when elements of the reactant wave function have passed through the potential well and are then propagating through the region where the product wave function is located.

Having setup our initial conditions, we will then develop a computer algorithm to replicate the Split Operator Method of propagating the initial wave function, $\Psi_R(x, 0)$, over a region of space with the predefined potential, $V(x)$. The result of this algorithm will serve as the propagated wave function in space and as time elapse scattering of the wave function as it passes the potential well, $V(x)$. We will allow the propagator to evolve in time and at each time step, we will generate a time based correlated function, $C(t)$, between the reactant wave function and the product wave function, by taking the integrated product of the two over position. Equation (1.2) illustrates this.

$$C(t) = \int \psi_R^*(x, t)\psi_P(x, 0)dx \quad (1.2)$$

⁵ Technically, the function is never truly non-zero as it is continuous, but for the purposes of the numerical approach the value held by the function is sufficiently small in comparison to the noise generated by numerical methods. In most of our cases the functional value was well below 10^{-10} when we say it is zero.

The correlated function will serve as our time signal of the scattering event. Then a numerical WDF will then be apply to the results from the time correlation in the following fashion.

$$W(t, \omega) = \frac{1}{\pi\hbar} \int C^*(t + \tau)C(t - \tau)e^{\frac{2i\omega\tau}{\hbar}} d\tau \quad (1.3)$$

Prior to generating the WDF of the correlation function, two outcomes will be generated to verify the accuracy of the numerical WDF generated. First, the correlation function will be multiplied by its complex conjugate and plotted versus time. Second, the correlation function will have an Inverse Fourier Transform applied to it to generate the correlation function in frequency space, $C(\omega)$, which in turn will be multiplied by its complex conjugate and plotted versus frequency. These plots will later be compared to the integrated projections of the WDF of the correlation function in order to verify that the WDF generated is accurate for the correlation function provided.

The correlation function, $C(t)$, will then be integrated in a computer algorithm to generate the WDF, $W(t, \omega)$, and in turn this will be the WDF of the scattering event between the propagating wave packet and the potential well. The WDF will then be plotted versus time and frequency. To verify the accuracy of the transform, $W(t, \omega)$ will then be integrated versus time to produce the WDF projection in frequency space, and integrated versus frequency, to produce the projection in the temporal domain. These projections will be plotted and compared to the plots of $|C(\omega)|^2$ and $|C(t)|^2$ generated previously. The two plots should appear to over lap for the WDF to be accurate. Figure

3 shows this comparison of $|\psi(x)|^2$ and $|\psi(k)|^2$ for the previously shown example of the WDF in figure 1 of the free particle.

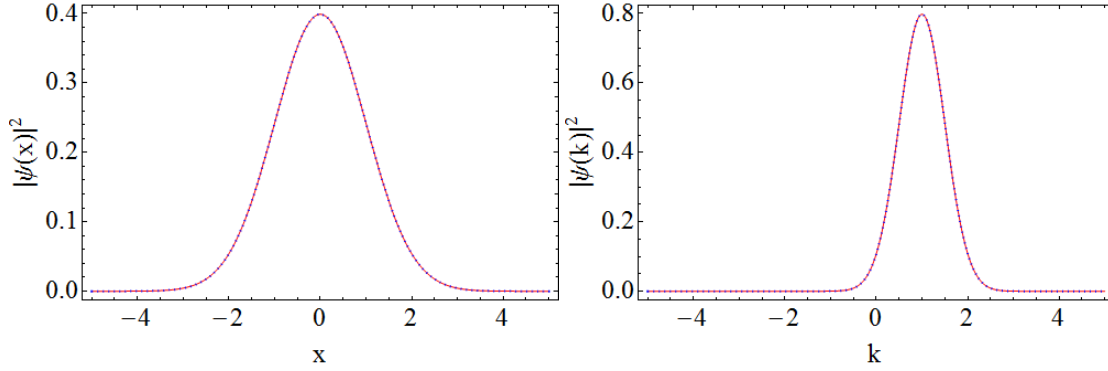


Figure 3. The comparison of the probability distribution in both position and momentum of free particle wave function at $\psi(x, 0)$. The solid red lines represents the solution derived by taking the modulus of the wave function and the blue dots represent the solution of the integrate projection of the WDF with the axes of interest.

With this approach we will first analyze the WDF for a square potential well. By using the square well we can compare the known attributes with the results of the WDF and determine if the WDF provides any insight into the physics going on within the scattering event. Additionally, we can compare the WDF result with a spectrogram of the correlation function.

In Section II, we will discuss giving a broader scope of the mathematical techniques used to generate the WDF such as the Fourier Transform, Split Operator Method, and the Free Particle Wave Function. A treatment of the square well will also be included for the purpose of comparison to the WDF. Section III will go over the technical aspects of the computer algorithm generated for this research in order to give an understanding of how the techniques were used and an explanation of the parameter decisions made. Section IV presents the results of the generated WDF for the various wells analyzed, followed by an analysis in Section V.

II. Background

2.1. Fourier Transform

A crucial component of research between position and momentum in quantum mechanics, as well as time and frequency, is the proper use of Fourier Transformations. Fourier Transformation is a process which transforms a complex-valued function of a real variable into another variable. [3] [4] A better way to look at this transformation is by viewing a function of any variable as vector of some magnitude and direction in an infinitely defined space of the variable. So if $f(x_1)$ is the value of the function at x_1 then in this vector view, $f(x_1)$ is the projection of f on the x_1 axis. Extending this logic to a continuous function which existed over the entire x domain, we would be able to describe a vector f to be in the infinite vector space of x . If this vector was then transported in a new vector space, with each new axis being related to a corresponding x -space axis by a phase shift, the f vector would have a new set of projections onto the new infinite vector space and would have a new shape in the new domain.

This is essentially how the Fourier Transform works between conjugate pairs of variables. For the conjugate pair of position and momentum; its relationship is given by the following: [5]

$$f(x) = \frac{1}{\sqrt{2\pi}} \int F(k) e^{ikx} dk \Leftrightarrow F(k) = \frac{1}{\sqrt{2\pi}} \int f(x) e^{-ikx} dx \quad (2.1)$$

The factor $\frac{1}{\sqrt{2\pi}}$ is used to normalize the functions as you transform between one domain, to the other, and back again. With that in place you can go back and forth between the two domains and always return to the original functions.

Another conjugate pair is time and angular frequency which is given by the same form as the equation (2.1) with the substitution of t for x and ω for k . By extension, this time/angular frequency pairing is also a time/energy pairing due to the DeBroglie relationship, $E = \hbar\omega$.

In order to analytically compute the Fourier Transform, the function must converge as the domain goes to its infinite limits. This poses a problem when you look at things in a discrete and finite frame of view. However, as long as the function value sufficiently goes to zero well before the end of the finite domain, a discrete form of equation will provide the correct transform for the original function.

2.2. Wigner Distribution Function

The development of quantum mechanics and its counter intuitive nature posed many problems for physicists in the early part of the 1900s. Classically, a system would be modeled and evaluated based on known characteristic values, such as the precise position of a billiard ball at an exact time, and from that information future outcomes could be stated with a fair amount of certainty based on the laws of classical dynamics. If you knew the position and momentum of a particle and the system⁶ it occupied then you knew not only everything that had happened to the particle, but what would happen to it given a universal knowledge of the system it occupied. Laplace is famously noted as having stated that the universe was composed of particles obeying Newton's laws and "once the interaction between these bodies is precisely known and the position and velocities of all the bodies at any given instant are known, these coordinates and

⁶ This state meant makes the broad assumption that the system is a non-interactive closed system with regard to the rest of the universe. More of a mental exercise than an actual case.

velocities are determined (through Newton's second law) for all time." [6] This comfortable determinism would soon be shaken by DeBroglie's Wave-particle Duality and Heisenberg's Uncertainty Principle.

However, this did not discourage some from approaching the new landscape of physics with some traditional notions. One of these physics was Eugene Paul Wigner⁷ who tried to tie in the traditional phase-space picture with what was being developed in the field of quantum mechanics and its force condition of quantum uncertainty. In 1932, he developed a distribution function as a means to study quantum corrections to classical statistical mechanics. Fundamentally, this quasi-distribution function generates a 2D surface in phase-space whose integrated projection on either axis will return the modulus of the wave function for that axis. Today this distribution function is called the Wigner Distribution, or the Wigner-Ville Distribution⁸, and is shown as equation (2.2) for the conjugate pairs of position and momentum.

$$W(x, p) = \frac{1}{\pi\hbar} \int \psi^*(x + y)\psi(x - y)e^{\frac{2ipy}{\hbar}} dy \quad (2.2)$$

Fundamentally, the distribution function is a Fourier Transform of a correlated wave function. An example of such a distribution function is given in figure 1. In figure 1, all the values of the distribution are positive, but it is entirely possible for the WDF to render negative values in the plot. The meaning behind this negative property of the distribution

⁷ Pál Jenő Wigner, his native Hungarian name, was born on November 17, 1902 in Budapest. He immigrated to the United States in 1930. He was a heavy contributor to Quantum Group Theory. He died on January 1, 1995. His notable relative is Paul Dirac, his brother-in-law by his first marriage.

⁸ After J. Ville who in 1948 rederived it as a quadratic (in signal) representation of the local time-frequency energy of a signal. It is additionally interesting to note that both Heisenberg and Dirac also derived this function, but missed its significance. [21] Also in 1949, José Enrique Moyal independently derived it. [20]

is unclear and makes it exceedingly difficult for one to interpret the WDF as a probability distribution in phase space.

Additionally, figure 2 depicts the comparison of the integration of the WDF along the momentum axis with the modulus wave function in its coordinate representation. This demonstrates that the WDF contains the information about the wave function in both coordinate space and momentum space.

So far we have examined the position-momentum WDF, but the WDF is not limited to that singular case. Any conjugate pair can have this technique applied to it and it is often used in the pairing of time and frequency such as shown in equation (2.3).

$$W(t, \omega) = \frac{1}{\pi\hbar} \int \psi^*(t + \tau)\psi(t - \tau)e^{\frac{2i\omega\tau}{\hbar}} d\tau \quad (2.3)$$

This is the form of the WDF we will use when examining the correlation of our scattered wave function over time. Except in our case $\psi(t)$ in equation (2.3) will be replaced by the calculated time correlation of the reactant and product wave function, $C(t)$, discussed later in Section 2.6.

2.3. Propagating Wave packet

Foremost in our analysis of the WDF as a signal processing tool is ability to accurately propagate our reactant wave function. As this function will serve as our propagating element in our initial setup and will be the wave function that will scatter with the quantum potential well in order to later produce the time signal by means of correlation with our product wave function. The uniqueness in the expression of the free particle wave packet is that as a wave function the function needs to be continuous over

all space, but still maintain its relative localization as it propagates in time much like a particle. Many authors discuss the development of this expression. [7] [6]

Schrödinger's Equation tells us that the time evolution of a wave function is the product of the initial wave function, an eigenfunction of the Hamiltonian, with the exponential of the Hamiltonian over time.

$$\psi(x, t) = e^{\frac{-i \mathbf{H} t}{\hbar}} \psi(x, 0) \quad (2.4)$$

Recall from our discussion on Fourier Transforms that a function of position can be defined as the integration of a function in momentum space, as shown in equation (2.1), and then equation (2.4) can be rewritten as

$$\psi(x, t) = e^{\frac{-i \mathbf{H} t}{\hbar}} \frac{1}{\sqrt{2\pi}} \int F(k) e^{ikx} dk \quad (2.5)$$

Since the free particle assumes that the potential component of the Hamiltonian is zero over all space, only the kinetic part remains which is also a function of momentum,

$T = \frac{(\hbar k)^2}{2m} = \hbar \omega$. Equation (2.5) then consolidates into the following

$$\psi(x, t) = \frac{1}{\sqrt{2\pi}} \int F(k) e^{i(kx - \omega t)} dk \quad (2.6)$$

However, $F(k)$, is time independent and by the same Fourier relationship can be given by the following

$$F(k) = \frac{1}{\sqrt{2\pi}} \int \psi(x, 0) e^{-ikx} dx \quad (2.7)$$

Substituting equation (2.7) into equation (2.6) we reach the following expression

$$\psi(x, t) = \frac{1}{2\pi} \int \int \psi(x', 0) e^{-ikx'} dx' e^{i(kx - \omega t)} dk \quad (2.8)$$

Since we want our initial wave function to have a relatively localized position we will use the time independent Gaussian wave function

$$\psi(x, 0) = \frac{1}{\delta^{1/2} (2\pi)^{1/4}} e^{ik_0 x} e^{-x^2/4\delta^2} \quad (2.9)$$

as our initial wave function in equation (2.8) and reach the following form

$$\psi(x, t) = \frac{1}{\delta^{1/2} (2\pi)^{5/4}} \int e^{i(k_0 x' - \frac{x'^2}{4\delta^2})} dx' \int e^{i(k(x-x') - \frac{k^2 \delta^2 t}{\tau})} dk \quad (2.10)$$

where $\tau = \frac{2m\delta^2}{\hbar}$. We now integrate equation (2.10) over all space and all momentum to

arrive at our final form of the free particle wave function

$$\psi(x, t) = \frac{1}{\sqrt[4]{2\pi} \delta^2} \frac{1}{\sqrt{1 + \frac{i\hbar t}{2m\delta^2}}} e^{\frac{-(x-x_0)^2}{4\delta^2} + i k_0 (x-x_0) - \frac{i\hbar t}{2m} k_0^2} e^{i \frac{\hbar t}{2m\delta^2}} \quad (2.11)$$

where x_0 is the initial center position of the wave packet, k_0 is the initial kinetic energy, δ is the initial spread of the wave packet in coordinate space, and m is the mass of the particle. Figure 4 depicts the time evolution of the real and imaginary component of the wave function.

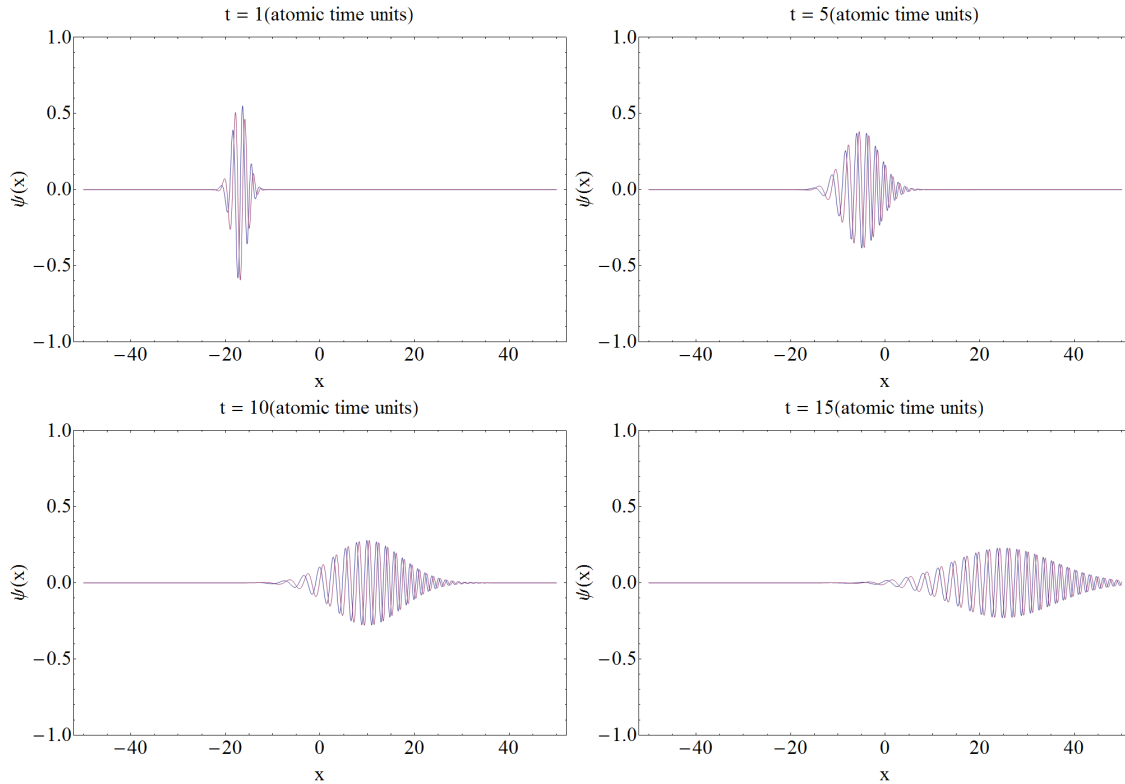


Figure 4. The time evolution of the real and imaginary components of a free particle with initial values of $x = -20$, $k = 3$, and a spread of 1.

As you can see, the wave function starts with a distinct position⁹ and spreads out over all space as time progresses. This is the expected outcome of the time evolution of the free particle. Initially, the probability of finding the particle in a set region is high, but as time progress the probability of location of the particle gets spread over an ever larger location.¹⁰ When we set $t = 0$ equation (2.11) simplifies down into,

$$\psi(x, 0) = \frac{1}{\sqrt[4]{2 \pi \delta^2}} e^{-\frac{(x-x_0)^2}{4 \delta^2} + i k_0 (x-x_0)} \quad (2.12)$$

⁹ Saying, “distinct position,” may be to strong of a statement. The particle location is as distinct as Heisenberg’s Uncertainty principle allows, but in terms of the entirety of space, the location is very localized.

¹⁰ Actually, the particle has a probability of being located at any point in the continuum of position space, but the beauty of the free particle wave function is that the overall Gaussian shape restricts the region of highest probability over a smaller region which only broadens with time.

Equation (2.12) is exactly equation (2.9) which you may recall was the time independent Gaussian wave function. This is not surprising as when you take the time dependent expression of the wave function and set $t = 0$ you should return to the time independent form of the expression. This form will serve as our initial wave function, but the time-dependent form will not function as our time propagator because it's Hamiltonian does not contain the elements of the potential well we wish to have the particle scatter upon as explored above.

2.4. Split Operator Method

Previously we demonstrated the form of the propagating wave packet wave-function when the Hamiltonian has no potential energy component. However, in our case we will be looking at examples where the potential is not zero everywhere. This would force us to re-exam our previous derivation for each Hamiltonian we wish to look at in order to derive the appropriate eigenfunction that showed the correct time based propagation. As we wish to exam a wide variety of wells, this would become a very laborious process and with possibility of finding no analytic solution.

Instead of developing a correct function for each Hamiltonian, we will be using the Split Operator Method to develop a time based wave function based on an input potential. The Split Operator Method [8] [9] is an outcrop of the Schrödinger Equation as show in equation (2.5). Split Operator Method takes the time dependent form of the Schrödinger Equation and rewrites the Hamiltonian Operator in terms of its component operators, $\mathbf{H} = \mathbf{T} + \mathbf{V}$. In this new form we can rewrite the argument of the exponential and a new form of the Schrödinger Equation appears as: [10]

$$\psi(x, t + \Delta t) = e^{-\frac{iV\Delta t}{2\hbar}} e^{-\frac{iT\Delta t}{\hbar}} e^{-\frac{iV\Delta t}{2\hbar}} \psi(x, t) + O(\Delta t^3) \quad (2.13)$$

The factor of $O(\Delta t^3)$ arises from the fact that \mathbf{T} and \mathbf{V} do not commute and the third term in equation (2.14) is not 1 as it is when applied to scalars. [11]

$$e^{ab} = e^a e^b e^{-\frac{1}{2}[a,b]} \quad (2.14)$$

In order to avoid issues with this $O(\Delta t^3)$ term, we will ensure that we make Δt sufficiently small in comparison to the total energy of the system we want to examine and we will assume that the last term is small enough, by the third power, to be considered zero. With the Schrödinger Equation now in the form given by equation (2.13), we can capitalize on the Fourier Transform to avoid further complexities of the \mathbf{T} and \mathbf{V} operators. By this I mean in coordinate space, the \mathbf{V} operator is merely, $V(x)$ or diagonalized in coordinate space, which makes the operation of

$$f(x, t) = e^{-\frac{iV(x)\Delta t}{2\hbar}} \psi(x, t) \quad (2.15)$$

a product of two functions. However, in coordinate space \mathbf{T} becomes harder to manage as shown in equation (2.16)

$$h(x, t) = e^{-\frac{i\frac{\delta^2}{\delta x^2}\Delta t}{\hbar}} f(x, t) \quad (2.16)$$

To avoid expanding the exponential into a Taylor Series and then applying the operator to the function, we can simply Inverse Fourier Transform, $f(x, t)$, into momentum space and make the result a simple product of two functions as before. As \mathbf{T} in momentum space is simply,

$$\mathbf{T} = T(k) = \frac{(\hbar k)^2}{2m} \quad (2.17)$$

which is to say \mathbf{T} is diagonalized in momentum space and then equation (2.16) can be rewritten as:

$$h(k, t) = e^{-\frac{i T(k) \Delta t}{\hbar}} f(k, t) \quad (2.18)$$

From that point we simply Fourier Transform back to the coordinate representation and compute the last product to arrive at $\psi(x, t + \Delta t)$. In repeating this process by using the resultant $\psi(x, t + \Delta t)$ as the new $\psi(x, t)$, the time evolution of the wave function can be generated in steps of Δt . Equation (2.19) shows the overall process:

$$\psi(x, t + \Delta t) = e^{-\frac{-i V(x) \Delta t}{2 \hbar}} FT \left[e^{-\frac{-i T(k) \Delta t}{\hbar}} FT^{-1} \left[e^{-\frac{-i V(x) \Delta t}{2 \hbar}} \psi(x, t) \right] \right] \quad (2.19)$$

2.5. Square Well Scattering

Understanding of the quantum square well is crucial to our analysis of the WDF of a scattered wave packet incident upon the well. Fortunately, the finite square well is a well know problem with multiple examples to pull from. [12] [6] [13] [7] By understanding its known attributes we will be better able to identify features of our resultant WDFs and make knowledgeable observations.

If we examine the scenario where we have a propagating wave which travels in the direction of x and experiences zero potential until a region of space, from $-a$ to a , where the potential is a negative constant value, we then have the case of a quantum square well. If we accept that a portion of the propagating wave will reflect off the first

boundary well and that some will pass through, we can then define the equation of the wave in the region before the well as:

$$\psi(x) = Ae^{ikx} + Be^{-ikx} \quad (2.20)$$

$$k = \frac{\sqrt{2mE}}{\hbar} \quad (2.21)$$

where A is the incident amplitude and B is the reflected amplitude. Within the well we can define the wave function as:

$$\psi(x) = C \sin lx + D \cos lx \quad (2.22)$$

$$l = \frac{\sqrt{2m(E + V_0)}}{\hbar} \quad (2.23)$$

On the far side of the well we can define the wave function as:

$$\psi(x) = Fe^{ikx} \quad (2.24)$$

In this case, k is the same as equation (2.21) and there is no reflected amplitude as we assume the wave is travelling from left to right. With these equations we impose two boundary conditions on the wave function. First that $\psi(x)$ is continuous and that $\frac{d\psi}{dx}$ also is continuous at the boundaries.

From that we can set up a system of equations that allows us to set the transmitted amplitude, F , in terms of the incident amplitude, A .

$$F = \frac{e^{-2ika}}{\cos 2la - i \frac{\sin 2la}{2kl} (k^2 + l^2)} A \quad (2.25)$$

We can then define the transmission coefficient of the well by using equation (2.25) in equation (2.26).

$$T = \frac{|F|^2}{|A|^2} \quad (2.26)$$

2.5.1. Transmission

The transmission coefficient is a function of energy; when equation (2.25) is applied to equation (2.26) what is left is an expression in terms of k and l , which they themselves, as show in equation (2.21) and (2.23), are functions of energy. Equation (2.27) demonstrates this.

$$T = \frac{1}{1 + \frac{V_o^2}{4\hbar\omega(\hbar\omega + V_o)} \sin^2 \left(\frac{2a}{\hbar} \sqrt{2m(\hbar\omega + V_o)} \right)} \quad (2.27)$$

In figure 5, we see this transmission coefficient plot over energies of the incident wave function and we can see that when energy increases, the degree of the transmission is increased.

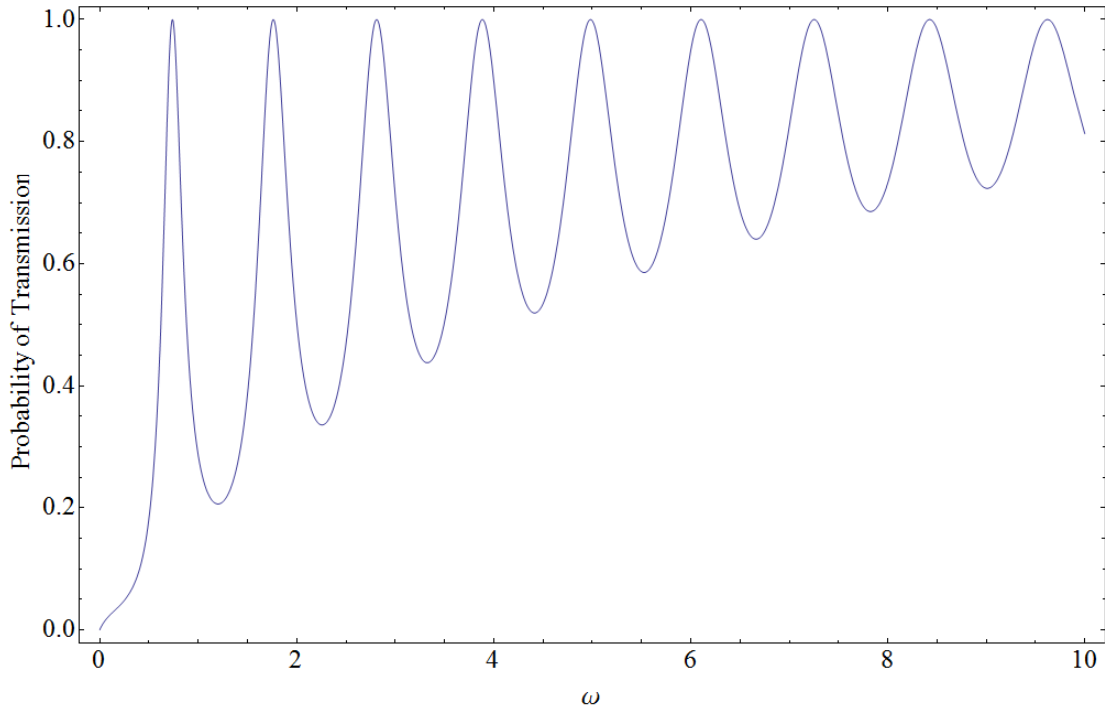


Figure 5. The transmission as a function of energy of a square well with depth, $V_o = 20$, and width, $2a = 20$.

You will also notice the sinusoidal shape of the curve as it moves towards 1. These peaks rise up to the value of total transmission before returning to the general arc of the curve. Since E is related to angular frequency by \hbar , these points represent frequencies of total transmission through the square well. At these frequencies/energies the square well is completely transparent to the particle.

The overall shape of the transmission coefficient is the same for all square wells, but varies in the degree at which the peaks rise up from the general arc of the function to 1 and in the spacing between these peaks (i.e. the spacing between peaks decreases as the well depth increases). In Merzbacher's analysis [7] of the square well, he defines a β

parameter to the square well that determines the degree of resonance given by the following:

$$\beta = \frac{\sqrt{2 m V_0}}{\hbar} a \quad (2.28)$$

More resonant wells are seen to have a larger β value and thus has a larger depth or width, or the particle has a larger mass, or a combination of all three.

2.5.2. Energy Levels

Additionally, the peaks of the transmission coefficient coincide with energies that cause the sine squared term to be a multiple of π .

$$\frac{2a}{\hbar} \sqrt{2m(\hbar\omega + V_0)} = n\pi \quad (2.29)$$

This forces the second term of equation (2.27) to be zero and we have total transmission.

If we solve for the angular frequency we get a quantized frequency which is the same as if the square well, had it been an infinite square well, and we are looking at energy levels V_0 above the bottom of the square well. Equation (2.30) expresses these angular frequency levels:

$$\omega_n = \frac{(n\pi)^2 \hbar}{2m(2a)^2} + \frac{V_0}{\hbar} \quad (2.30)$$

2.6. Time Correlation Function

So far we have examined the propagation of a reactant wave function in conjunction and its scattering off a potential well, but not a means of recording the result of the scattering as a function of time. For that we must correlate our wave function with

a stationary wave function at a given position beyond the well from the starting point of our propagating wave function. [14]

$$C(t) = \int \psi_R^*(x, t)\psi_P(x, 0)dx \quad (2.31)$$

The correlation function enables us to see what elements, the amplitudes of the real and imaginary components, of the propagating wave function are passing a certain position as time evolves. Additionally, we will also gain information about frequencies that pass through the stationary point based on the Fourier relationship between time and frequency.

2.7. Atomic Units

As we explore the interactions of the propagating wave function with the imposed well we will use the atomic unit system for our numerical values. This is a common unit system for analysis of events at the atomic level and is often used in Chemical Physics research. The main benefit it will serve in this research is in reducing many of our constants values to 1 such as mass, the mass of an electron in this case, and Planck's constant. While the numerical approach is indifferent to the units used, the atomic unit system gives us a more intuitive scale upon which to view the results of our computational model. Table 1 shows a comparison of the units in the atomic unit system with those in the International System of Units (SI)

Table 1. Atomic Units System [15]

Quantity	Name	Symbol	SI Value
mass	electron rest mass	m_e	$9.109 \cdot 10^{-31}$ kg
length	Bohr radius	$a_0 = \frac{\hbar}{m_e c \alpha}$	$5.291 \cdot 10^{-11}$ m
charge	elementary charge	e	$1.602 \cdot 10^{-19}$ C
angular momentum	Reduced Planck's constant	$\hbar = \frac{h}{2\pi}$	$1.504 \cdot 10^{-34}$ J s
energy	Hartree energy	$E_h = m_e c^2 \alpha^2$	$4.359 \cdot 10^{-18}$ J
electrostatic force constant	Coulomb's constant	$\frac{1}{4\pi\epsilon_0}$	$8.987 \cdot 10^9$ N m ²
time		$\frac{\hbar}{E_h}$	$2.418 \cdot 10^{-17}$ s
velocity		$\frac{a_0 E_h}{\hbar}$	$2.187 \cdot 10^6$ m s ⁻¹

III. Numerical Approach

3.3. Fast Fourier Transform

Previously, we discussed the process of Fourier Transforming one continuous function in a position (or time) domain into a continuous function in a momentum (or frequency/energy) domain. However, since we are taking a numerical approach to the propagation of a free particle scattering off of a square well, we will not have a continuous domain to work with, but the inside of a very controlled finite domain. This will force us to perform a Discrete Fourier Transform when we seek to perform the operations given by equation (2.19). All numerical computation where programmed into FORTRAN77.

It would be possible to take the integral form shown in equation (2.1) and revert it into a Riemann Sum expression with a Δx of our choosing

$$F(k_i) = \sum_{x=x_1}^{x_n} \Delta x * f(x) * e^{ik_ix} \quad (3.1)$$

This would be able to discretely transform $f(x)$ on the range $x_1 \rightarrow x_n$ into $F(k_i)$. This would be repeated for every $F(k_i)$ over a pre-determined range and would provide the Fourier Transformed function. Provided that the ranges chosen are sufficiently large such that non-zero portions of the functions are not excluded in either domains, then this Discrete Fourier Transform will be highly accurate.

This approach however has a drawback when it comes to the computational time it takes to perform these procedures. “The interpolation of $2m$ data points by the direct

calculation technique requires approximately $(2m)^2$ multiplications and $(2m)^2$ additions.”

[16] Fortunately, J.W. Cooley and J.W. Tukey developed a numerical process that reduced the number of multiplications and additions to $(m \log_2 m)$, called the Fast Fourier Transform. The only requirement imposed by this technique is that the position (time) domain and the momentum (frequency) domain must share the same number of grid points, and those grid points have to be on the order of 2^N . [16] [3]

Due to its efficiency there are many available Fast Fourier Transform subroutines available in most every computational programming language. We implemented a 1 dimensional Fast Fourier Transform into our code in order to perform the transforms need in equation (20) and also for additional transforms into momentum space for calculating the norm of k at each time step in our program.

3.4. Aliasing

One of the issues encountered with our use of discrete FT and the process efficient FFT was one of Aliasing. Aliasing essentially occurs when a continuous signal is sampled and reconstructed on a fixed range allowing for the development of distortions or artifacts to be represented. In a purely mathematical FT, the integration of the input signal would be over the entire time domain, i.e. from $t = -\infty$ to $t = \infty$. However, doing such integrations numerically is impossible, so we imposed the restriction that over a short window the signal would be zero at the imposed boundaries of the window and therefore the integration could be imposed over those limits. While these imposed restrictions do work to transform the function from time to frequency, they have to be handled properly or they will create distortions or artifacts.

The reason is that when this windowed regime of the function is generated, it actually creates an infinite series of these windows that follow one another in the domain of the space being transformed into. Each of these windows is a replicate of the previous, starting where the previous window ended. If an arbitrary length is chosen over which to measure and describe the domain being transferred into, then there is the risk of recording more than one of these windows and creating a transform that actually contains multiples of the true transform.

These distortions can be avoided by imposing a range restriction on the domain being transformed into. This restriction is called the Nyquist Frequency and is shown in equation (3.2). [4] [3] [17]

$$\omega_{max} = \frac{\pi}{\Delta t} \quad (3.2)$$

This restriction, while aiding in eliminating distortions and artifacts, forces us to be very careful in our choice of Δt . We are already forced to choose a Δt that is small in comparison to the energies of the system we are investigating due to the use of the Split Operator Method, but now we must be careful not to make our ω_{max} too large or the $\Delta\omega$ too big to be a meaningful representation of $|\psi(\omega)|^2$, but also ensuring ω_{max} included all of the information of $|\psi(\omega)|^2$. In a case involving $x \rightarrow k$ transforms, we are further burdened by the FFTs requirement that both domains be characterized by 2^N number of points to function properly. This adds the further balancing act of ensuring k_{max} includes all the appropriate information of the kinetic energy from the scattering, even in addition to wanting both Δx and Δk to be small enough to properly characterize the

functions in those domains. Table 2 shows this imposed restriction and its resulting values used in the FORTRAN 77 code generated for this research.

Table 2. Comparison of grid sizes and grid step sizes for Discrete Fourier Transforms

Conjugate Pairs ($a \rightarrow b$)	a_{max}	Δa	b_{max}	Δb^{11}	#points
$x \rightarrow k$	100	.09766	32.16991	.03142	2048
$t \rightarrow \omega$	99.99	.09	34.90659	.03142	1111

It should be noted that Δt was actually .01 in the Split Operator Method portion of the code but was down sampled, as explained previously, to .09 to save time in the processing of the WDF portion of the code. This value of .09 served as the value of Δt for all transforms of $t \rightarrow \omega$ in the code generated and is why it is displayed as the delta term in the table above.

3.5. Absorbing Boundaries

Since we are performing discrete transforms over a fixed regime of space, we run a similar risk to the aliasing described previously. If the wave function is allowed to propagate to the point where elements of the function pass the right side of our imposed window, we will see the return of those elements at left side which will interact with elements still in the window and distort our wave function. In order to avoid this we need to ensure that the wave function goes to zero as it reaches the end of the special regime. To do this we will add an imaginary term to our potential function that will be localized to the edges of our special window. [18]

¹¹ It was not intended for Δk and $\Delta \omega$ to match, but was the unexpected outcome of the values used.

$$V_{total}(x) = V_{int}(x) + iV_{abs}(x) \quad (3.3)$$

When this term is placed into the potential exponential of equation (2.19), we see the following result

$$e^{-\frac{iV\Delta t}{2}} \psi(x, t) = e^{-\frac{iV_{total}\Delta t}{2}} \psi(x, t) \quad (3.4)$$

$$e^{-\frac{iV\Delta t}{2}} \psi(x, t) = e^{-\frac{i(V_{int}+iV_{abs})\Delta t}{2}} \psi(x, t) \quad (3.5)$$

$$e^{-\frac{iV\Delta t}{2}} \psi(x, t) = e^{-\frac{(iV_{int}-V_{abs})\Delta t}{2}} \psi(x, t) \quad (3.6)$$

$$e^{-\frac{iV\Delta t}{2}} \psi(x, t) = e^{-\frac{iV_{int}\Delta t}{2}} e^{-\frac{V_{abs}\Delta t}{2}} \psi(x, t) \quad (3.7)$$

Provided that $V_{abs}(x)$ is negative, the second term of equation will serve to dampen the wave function multiplied with it. Additionally, to ensure the absorbing boundary potentials do not drastically dampen the wave function to the point of altering it within the special window, it is best to use a function that gradually applies the negative potential. We used a simple Gaussian, depicted in equation (3.8), to accomplish this.

$$V_{abs}(x) = Ae^{-\left(\frac{x-x_{min}}{b}\right)^2} + Ae^{-\left(\frac{x-x_{max}}{b}\right)^2} \quad (3.8)$$

In our research we set $A = 1$ and $b = 5$ for our absorbing boundary conditions.

Figure 6 depicts the interaction of the propagating free particle with one of the absorbing boundary function.

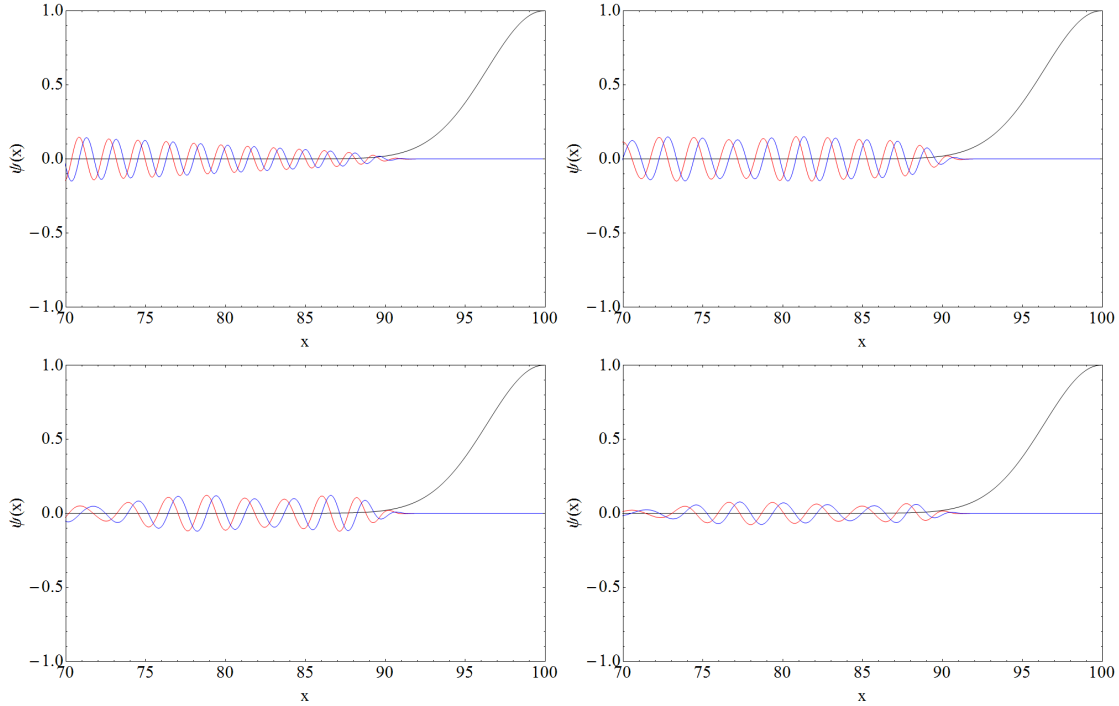


Figure 6. A propagating wave function incident on absorbing boundary potential

3.6. Free Particle Propagation

As explained in Section 2.4, the need to pick a sufficiently small Δt in order to avoid complications with the additive term in equation (2.13) was paramount. So in order to test the results produced from our numerical propagator we need to compare them with known analytic solutions of the same conditions. Since we have already derived the form of the free-particle wave function, we have an expression with which to perform one of our first comparisons. Since the free-particle Hamiltonian has no potential contribution, this comparison serves to analyze whether the kinetic component of our propagator is functioning accurately. By checking the application of equation (2.19) in our numerical code against a case solely comprising of one part of the Hamiltonian we ensure that later verification steps and issues that may be found with

those verifications are not attributes of the kinetic part of the Hamiltonian. Figure 7 shows the comparison between the numerical result and the analytic answer for a free-particle propagation derived in Section 2.3 and, as you can see, they are in agreement.

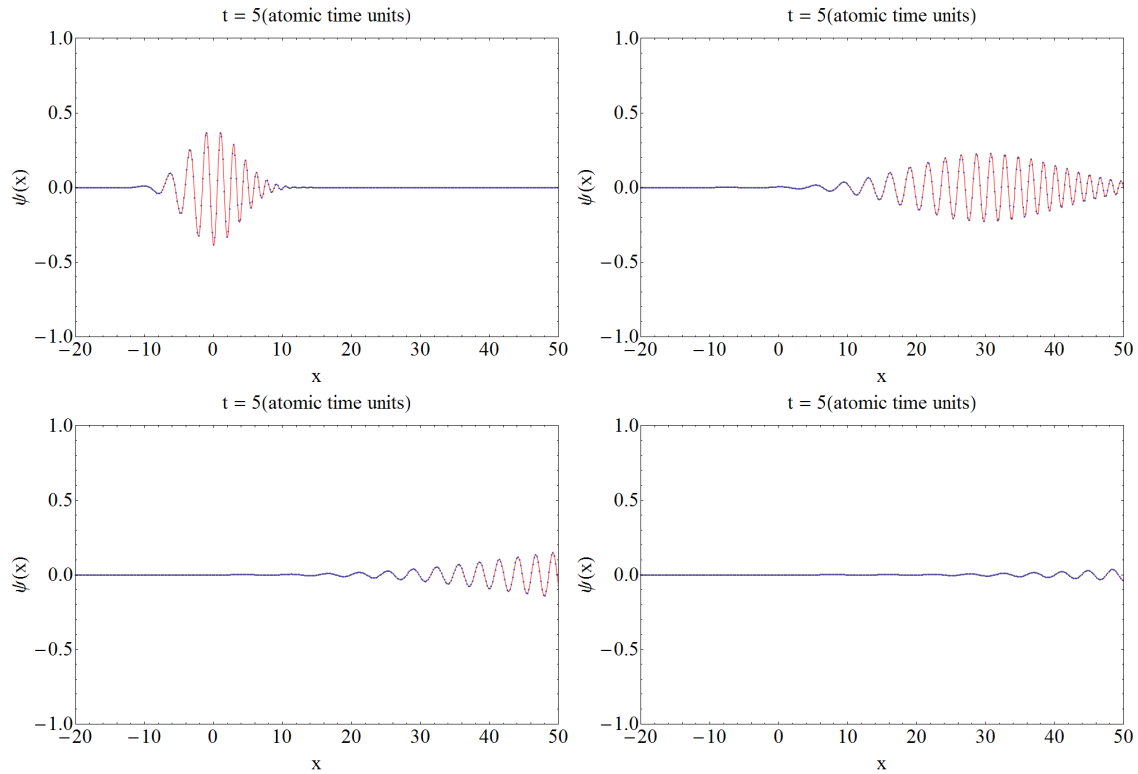


Figure 7. Comparison of the analytical form of a free particle wave function with the results of the split operator method. The blue dots represent the real part of the wave function as generated from the split operator method. The lines connecting the dots represent the analytical result of the real part of the wave function. The reason the wave function appears to leave the window and not cycle round again as discussed in this section is that the graphical depiction only shows a narrow portion (-20 to 50) of our x domain.

3.7. Coherent State of a Harmonic Oscillator

After reviewing the accuracy of our propagator to a Hamiltonian with no potential component, we then need to look for an analytic wave function for a Hamiltonian with both kinetic and potential contributions to use as a comparison for our propagator. The

wave function we utilized for this comparison was the Coherent State of the Quantum Harmonic Oscillator [13] given in the equations below

$$\psi(x, t) = e^{i\theta_\alpha} \left(\frac{m\omega}{\pi\hbar}\right)^{1/4} e^{-\frac{i\omega t}{2}} e^{\frac{i\langle P(t)\rangle}{\hbar}} e^{-\left(\frac{x-\langle X(t)\rangle}{2\Delta x}\right)^2} \quad (3.9)$$

$$\langle X(t)\rangle = \sqrt{\frac{2\hbar}{m\omega}} (\text{Re}[\alpha_0 e^{-i\omega t}]) \quad (3.10)$$

$$\langle P(t)\rangle = \sqrt{2m\hbar\omega} (\text{Im}[\alpha_0 e^{-i\omega t}]) \quad (3.11)$$

$$e^{i\theta_\alpha} = e^{\frac{(\alpha^*(t))^2 - (\alpha(t))^2}{4}} \quad (3.12)$$

$$\alpha(t) = \frac{1}{\sqrt{2}} \left(\beta x(t) + \frac{i}{\hbar\beta} p(t) \right) \quad (3.13)$$

$$\alpha_0 = \frac{1}{\sqrt{2}} \left(\beta x(0) + \frac{i}{\hbar\beta} p(0) \right) \quad (3.14)$$

The expression is the eigenfunction for the following Hamiltonian

$$H(x) = -\frac{\hbar^2}{2m} \frac{d^2}{dx^2} + \frac{1}{2} m\omega^2 x^2 \quad (3.15)$$

This is clearly a robust and complicated expression for the propagation of a wave function bound within a quantum harmonic oscillator potential. As such, careful accounting needs to be applied when generating the analytic result for our comparison.

3.7.1. Ground State

We first look at the simplest case of the Coherent State, $x(0) = 0$ and $p(0) = 0$, as a comparison for the propagated wave function given by our code. This is known as the ground state of the quantum harmonic oscillator. In this state, the wave function

looks very similar to the ground state of the infinite square well and its real and imaginary components oscillate at a $\frac{\pi}{2}$ phase shift from each other. Figure 8 shows the comparison between the numerical result and the analytic answer for the ground state coherent function and, as you can see, they are in agreement.

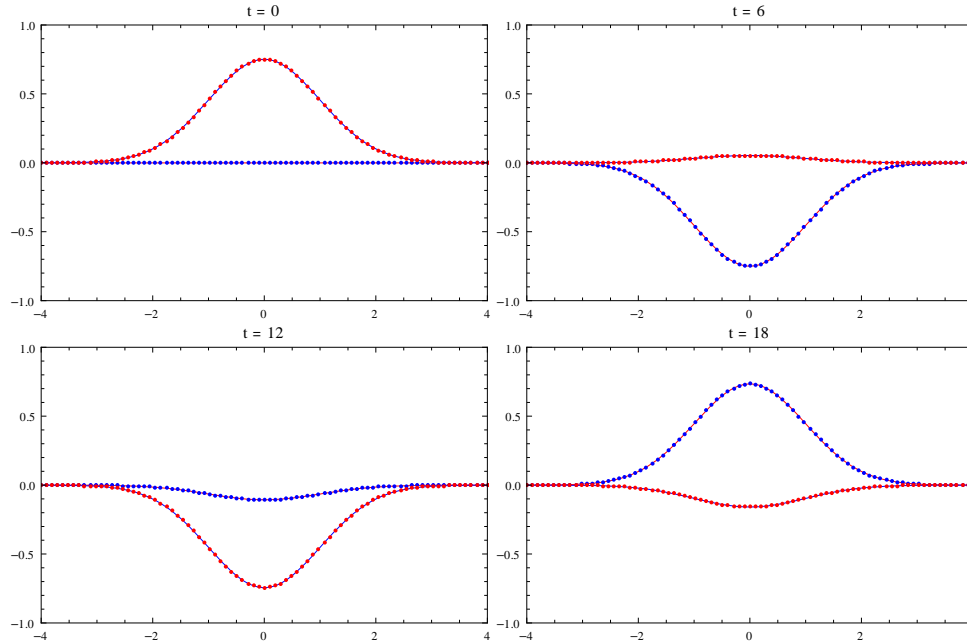


Figure 8. Comparison of the Coherent function ground state with the results from the split operator method. The blue dots represent the imaginary part of the wave function and the red dots represent the real part of the wave function as generated from the split operator method. The lines connecting the dots represent the analytical result and the colors are the converse for distinction between the lines and dots. In the analytical case the red line represents the imaginary part and the blue represents the real part.

The comparison of the free-particle propagation and the propagation of the ground state coherent function provide a sufficient check to determine whether the numerical propagator of equation (2.19) is working accurately. Future applications of the propagator will only need to apply a sufficiently small Δt , in keeping with the total

energy of the system being analyzed, to provide an accurate representation of the time propagation of the wave function.

3.8. Discrete Wigner Distribution (DWD) Function

Just as we had to modify our approach to Fourier Transforms based on the discrete nature of our numerical approach, so to do this we have to revisit the WDF given in equation (1.1) and apply it in a discrete fashion. In order to accomplish this we have to review the inner workings of the WDF. Fundamentally, the WDF is a Fourier Transform of a correlated function in time. If we break the WDF into a process of discrete correlation and a process of discrete Fourier Transformation we are half way done, given what we have already discussed in Section 3.3 and 3.4.

The process of correlation in the DWD essentially shifts the function, one function of time from the bottom to the top of a scale in τ space, while a conjugate function of the same time function is simultaneously shifted from the top to the bottom of τ space. With each shift in τ the product of the two functions is taken and this builds up the correlated function of time. If these functions of time are localized, that is to say they only have relatively non-zero values over a fixed region of time, then the value of the correlation will only have non-trivial values in the region of $-t_{max} \leq \tau \leq t_{max}$ where t_{max} is the last value of time for which the functional value is non-trivial. This process can be discretely accomplished numerically so that the only step left is to combine this process with the process of Fourier Transforming the correlated function in τ space into angular frequency space for all values of t .

3.9. Down Sampling

Down Sampling became a necessary component of our FORTRAN 77 code for several reasons. In wanting to explore square wells with strong resonant features we were forced to modify the square well in one of two ways; first being to increase the width and second being to increase the depth. Increasing the width of the well would require constant movement of the starting position of the wave packet further to the left of the well to avoid starting the computations with either the reactant or product wave function overlapping the location of the well. This would force us to continually readjust the domain range of x to avoid having the initial wave function located in areas that did not have zero value for the potential, be it from the well itself or from the absorbing boundary conditions, which would disrupt the initial state. Additionally, this would also run the risk of diminishing the k domain, due to the correlation between the x and k imposed by the FFT, to the point that it may not include all the kinetic energy values produced by the scattering.

Altering our well depth also imposed complications as it required that reduction in our time step to be able to satisfy the imposed restriction of the Split Operator Method. However, every time we decrease the time step of our propagator the length of the correlation array is increased over a fixed time interval. That is to say is we subdivide a length of time of 10 by intervals of 1 we end of up with 10 data points, but is we subdivide by .1 we end up with 100 data points. In turn, this input correlation array would increase the number of cycles the DWD would have to perform. Table 3 depicts

this relationship between the input array and the number of calculations the DWD would have to perform for a non-down sampled array.

Table 3. Down sampling values

Δt	C(t) array length	# of DWD cycles	Fraction of .09
.5	200	16,040,000	.00585
.1	1,000	2,001,000,000	.72926
.09	1,111 ¹²	2,743,895,583	1
.05	2,000	16,004,000,000	5.83259
.01	10,000	2,000,100,000,000	728.92715

The arrays depict a total time of 100 and the inclusion of .09 was done to show the attributes for the value later utilized.

We decided to forgo altering the well width and instead focused on changing well depths, but to avoid the calculation issues of a smaller Δt , the correlation array was down sampled by a factor of 9 which, as demonstrated above, made the total time approximately $\frac{1}{729}$ the actual time needed to generate a DWD at that time step. As a means of comparison, a DWD with the .09 step takes about 20 minutes. The same DWD with a .01 time step would take approximately 10 days¹³.

¹² In this case the time length is 99.99 as in our code that correlation was computed for $t = .09$ to $t = 100$. The instance of $t = 0$ was disregarded as by construction the correlation function would be zero at this point.

¹³ The results obtained from the 20 minute trials were sufficient enough in the analysis to retain all susceptible information of the WDF that any increase in granularity would add no benefit and cost excessive time.

IV. Results

In this section a large portion of the results obtained from the code and methods described in Sections II and III are displayed for the benefit of the reader. Additional results are displayed in Appendix A. The results are presented in such a way as to give the reader an appreciation of the outcomes of the modeling and simulations performed while saving all discussion of analysis and interpretations for Section V.

4.1 Correlation Function

The primary goal of this research was to generate a Wigner Distribution of the time correlation function, given by equation (1.2), between a reactant and product wave function. As such it is necessary to demonstrate the resulting calculated correlation function obtained via the Split Operator Method, already discussed previously, before moving on to the resulting Wigner Distributions obtained. Figure 9 shows such a correlation function generated after a reactance wave function has passed through a quantum square well of depth $20E_h$ and width of $a = 10\alpha_0$.

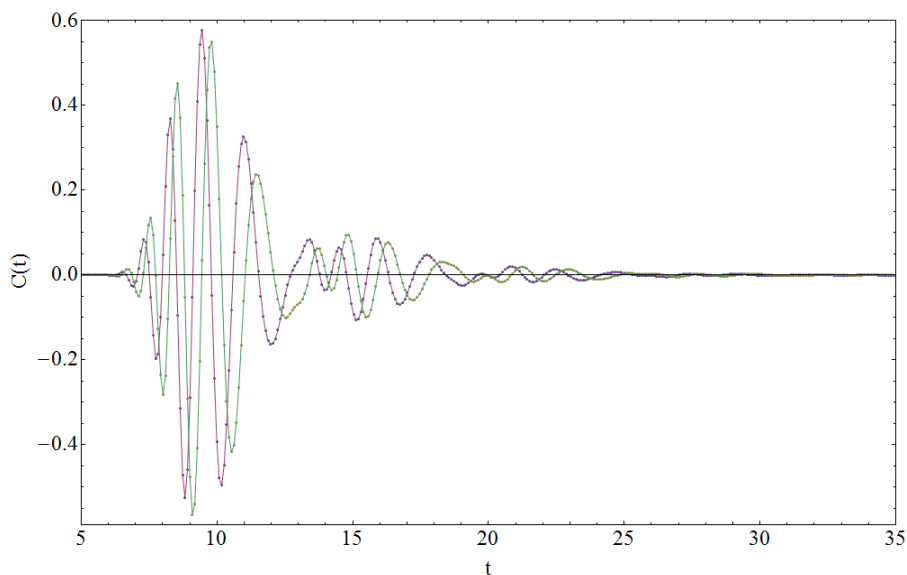


Figure 9. A correlation function, both its real and imaginary components, generated by the Fortran 77 code utilizing the Split Operator Method. Though only displayed from $t = 5$ to $t = 35$ the correlation function was captured for $t = 0.09$ to $t = 99.99$

As you can see from figure 9 the sampling interval, as discussed in the previous section, provide more than sufficient data points to accurately depict the function. Additionally, the correlation function it given sufficient amount of time to reduce to zero as show in figure 9 which only shows a window of the function from $t = 5$ to $t = 35$ in order to show depth of features in the graph. The true length of the correlation function, as mentioned in the previous section goes from $t = .09$ to $t = 99.99$.

4.2 Wigner Distribution Plots

Using the method and code described in Sections II and III respectively, we were able to generate Wigner distribution plots for a variety of well depths and well shapes. We, of course, first developed WDF plots for a range of square well depths. First the series between well depths was kept small, going from a value of 2 to a value of 8 by increments of 2. After that point, steps of 20 were used in order to reach levels which would produce higher levels of resonant features. After the full range of square well DWDs were generated the same series of well depths were applied to wells of differing shapes (triangular, circular, and Gaussian). As means of a baseline for our review of the WDF plots generated, figure 10 shows the WDF plot for a propagation free particle with no well to scatter upon.

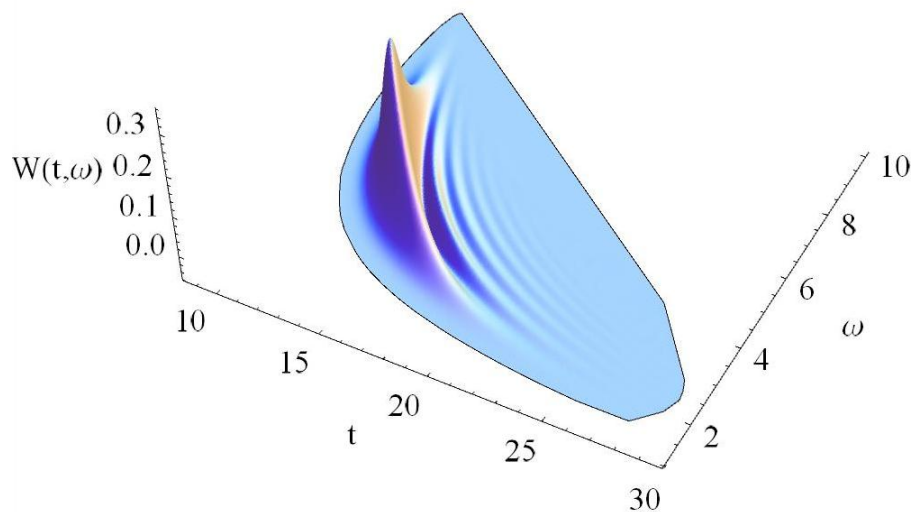


Figure 10. The WDF of a free particles correlation function

The unique features in figure 10 are interesting in and of themselves and provided the overall characteristic seen in many of the Wigner Distribution Plots for cases where a quantum potential well was present. In all cases the primary large mountain like feature seen in figure 10 is present along with the subsequent smaller L-shaped ridges. These ridge lines represent large portions of the reactant wave function correlation with the product wave function. Since we set out initial momentum of reactant wave function relatively large in order to avoid spreading the reactant wave in the negative direction we gain the effect of supplying a large amount of initial energy into the correlation and thus in all of our Wigner Distributions this very large primary peak is present.

We have included the WDF plots of the square wells and circular wells in this section. Appendix A displays the results of the triangular and Gaussian wells due to their lack of structure. A full analysis of these results is found in Section V.

As described in Section 2.5 of the square well scattering, the potential for a square well is a set of functions as show in equation (4.1)

$$V(x) = \begin{cases} -V_0, & -a < x < a \\ 0, & |x| > a \end{cases} \quad (4.1)$$

This is the form used for the V_{int} term of equation (3.3).

Since the potential is discretely defined, the potential is an approximation of the square well. The smaller we make Δx , the closer we make the approximation to a true square well, but ultimately the numerical process can never truly replicate the piecewise function described in equation (4.1). Fortunately the distortion is not large enough to cause issue in our data with the Δx we have selected, $\Delta x = .0976$.

4.2.1. Square Well with depth $V_o = 2, 4, 6, \& 8 E_h$

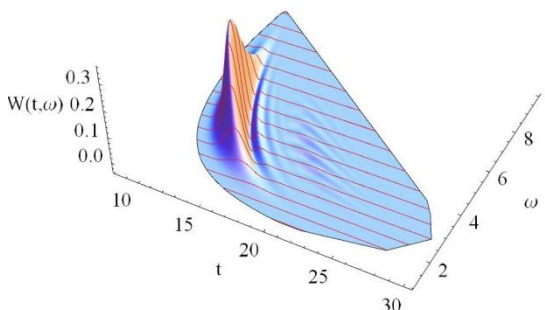


Figure 11. Depiction of a WDF plot generated from the time correlation function of a reactant wave function scattering through a quantum potential well of $2E_h$. The red lines indicate frequencies of total transmission that correspond to a well of that depth.

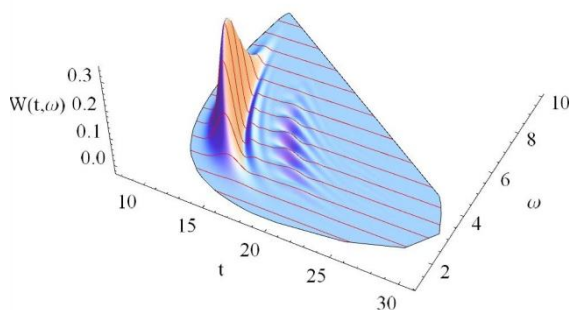


Figure 12. Depiction of a WDF plot generated from the time correlation function of a reactant wave function scattering through a quantum potential well of $4E_h$. The red lines indicate frequencies of total transmission that correspond to a well of that depth.

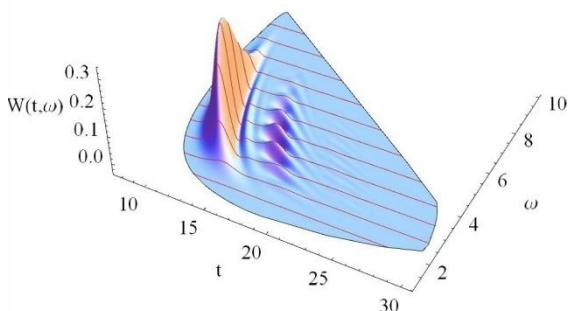


Figure 13. Depiction of a WDF plot generated from the time correlation function of a reactant wave function scattering through a quantum potential well of $6E_h$. The red lines indicate frequencies of total transmission that correspond to a well of that depth.

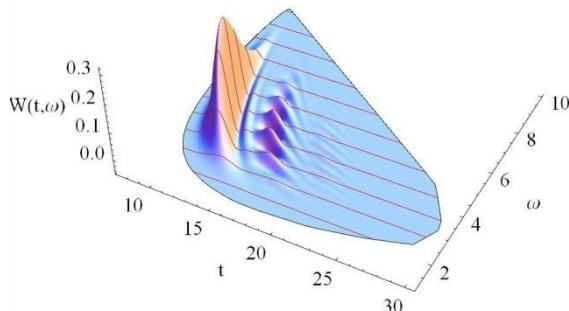


Figure 14. Depiction of a WDF plot generated from the time correlation function of a reactant wave function scattering through a quantum potential well of $8E_h$. The red lines indicate frequencies of total transmission that correspond to a well of that depth.

4.2.2. Square and Circular Well with depth $V_0 = 10, 20, 40, 60, \& 80 E_h$

The FORTRAN 77 code generated was tailored to the well width, $2a$, of 20 (atomic units) for the square well. When the code was modified to examine the circular well the following equation was used

$$V(x) = \begin{cases} -\sqrt{V_0^2 - \frac{V_0}{a}x^2}, & -a < x < a \\ 0, & |x| > a \end{cases} \quad (4.2)$$

This is the form used for the V_{int} term of equation (35). In this form the circular well maintains the same overall spacing in x as the square well did, so that the new potential can simple be substituted in the pre-existing FORTRAN 77 code.

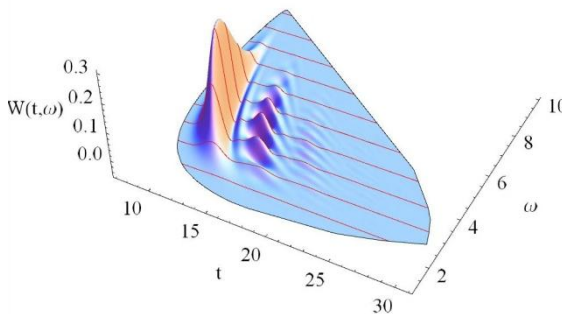


Figure 15. Depiction of a WDF plot generated from the time correlation function of a reactant wave function scattering through a quantum square well of $10 E_h$. The red lines indicate frequencies of total transmission that correspond to a well of that depth.

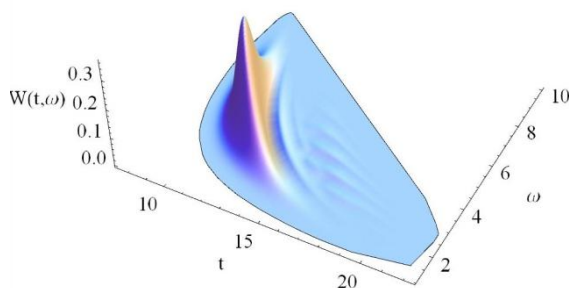


Figure 16. Depiction of a WDF plot generated from the time correlation function of a reactant wave function scattering through a quantum circular well of $10 E_h$.

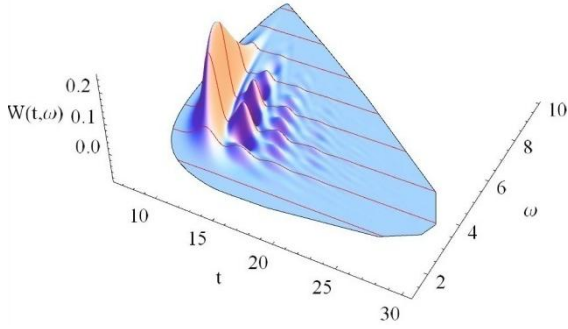


Figure 17. Depiction of a WDF plot generated from the time correlation function of a reactant wave function scattering through a quantum square well of $20 E_h$. The red lines indicate frequencies of total transmission that correspond to a well of that depth.

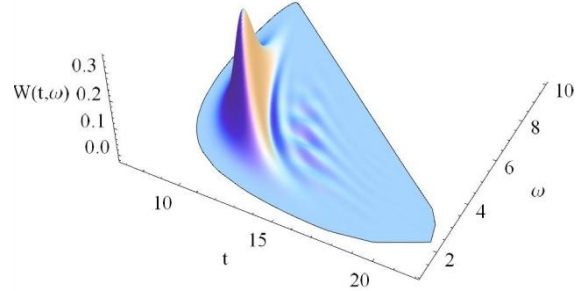


Figure 18. Depiction of a WDF plot generated from the time correlation function of a reactant wave function scattering through a quantum circular well of $20 E_h$.

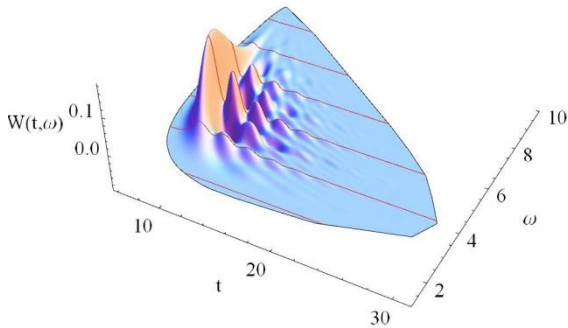


Figure 19. Depiction of a WDF plot generated from the time correlation function of a reactant wave function scattering through a quantum square well of $40 E_h$. The red lines indicate frequencies of total transmission that correspond to a well of that depth.

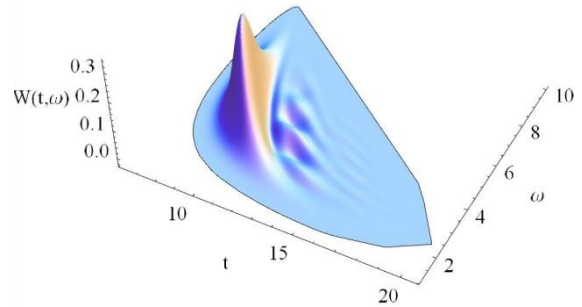


Figure 20. Depiction of a WDF plot generated from the time correlation function of a reactant wave function scattering through a quantum circular well of $40 E_h$.

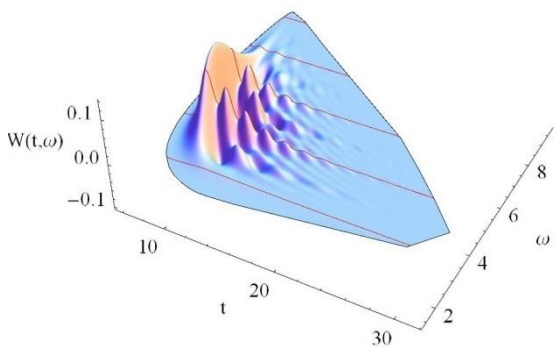


Figure 21. Depiction of a WDF plot generated from the time correlation function of a reactant wave function scattering through a quantum square well of $60 E_h$. The red lines indicate frequencies of total transmission that correspond to a well of that depth.

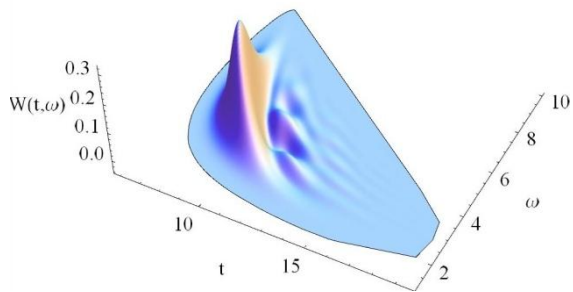


Figure 22. Depiction of a WDF plot generated from the time correlation function of a reactant wave function scattering through a quantum circular well of $60 E_h$.

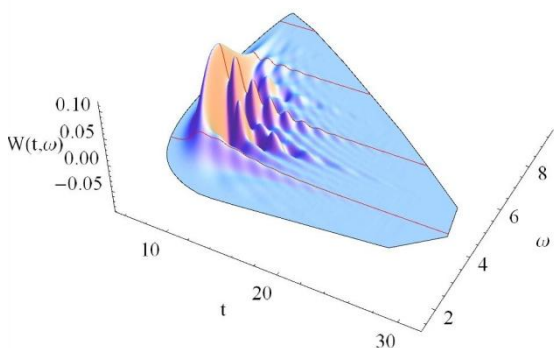


Figure 23. Depiction of a WDF plot generated from the time correlation function of a reactant wave function scattering through a quantum square well of $80 E_h$. The red lines indicate frequencies of total transmission that correspond to a well of that depth.

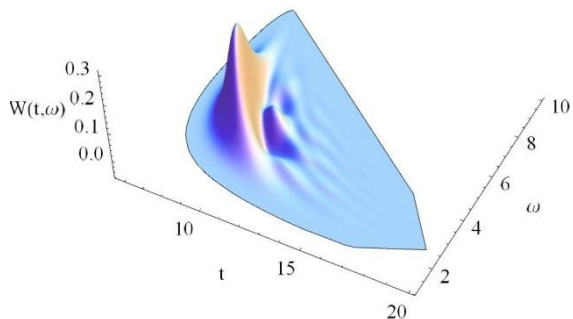


Figure 24. Depiction of a WDF plot generated from the time correlation function of a reactant wave function scattering through a quantum circular well of $80 E_h$.

V. Analysis

In viewing the results of the square well and comparing those results with known attributes of that same well, many noteworthy features begin to appear in our WDF plots. We will examine these attributes in the case of a square well with a depth of $20E_h$ unless otherwise noted in the discussion. This is not to say that these features are not present in all cases, but the example gives us a good case where we do not run into extremes of all the features, which can obscure the individual attributes.¹⁴

5.1. Transmission Coefficients

As discussed in Section 2.5.1 a square well allows for certain energy bands to pass through as if the well were transparent. When we take the integrate projection of the WDF generated from the scattering event towards the frequency axis, we get the probability distribution of the frequency of our correlation function from that scattering event. Figure 25 shows the integrate projection of the WDF for the square well of $V_0 = 20$ and $a = 10$.

¹⁴ This also helps us from diluting the results with multiple graphical plots restating the point.

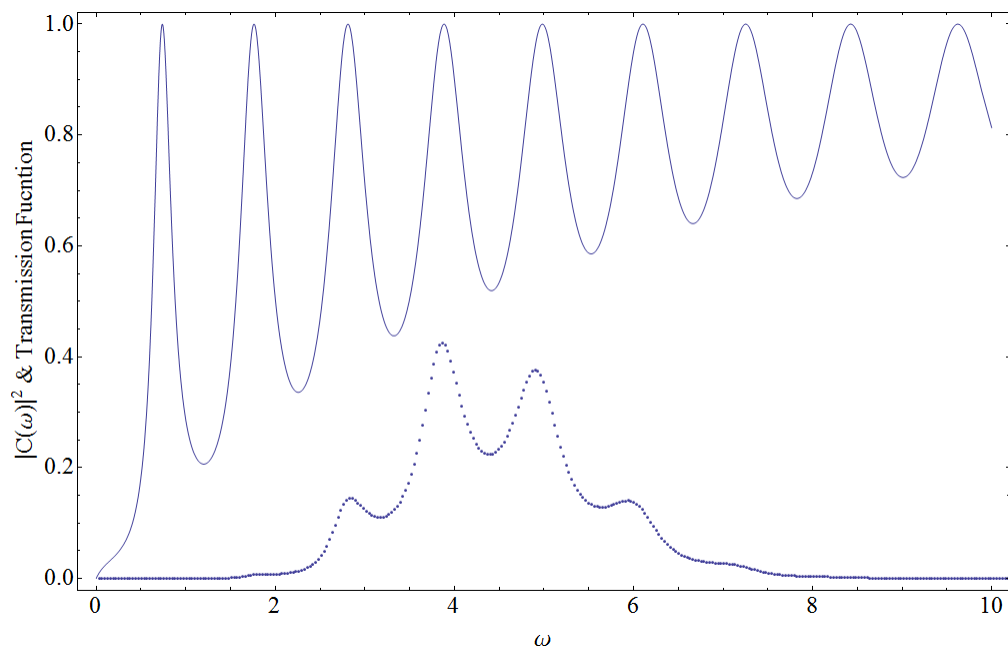


Figure 25. The integrated projection of the WDF in frequency is given by the blue dots and the transmission function of a square well of width $2a = 10$ and $V_0 = 20$ is given by the solid blue line.

By inspection, the distribution has an overall Gaussian shape. This is due to the fact that the reactant and product wave functions were Gaussian by construction¹⁵. Within the overall Gaussian shape there appears to be protruding peaks at specific values of frequency. These peaks coincide when compared to the known transmission peaks of the square well. Further, the overall Gaussian function is given by the modulus of the frequency correlation of the two initial wave functions when no well is present

$$|C(\omega)|^2 = C^*(\omega)C(\omega) \quad (5.1)$$

¹⁵ If we had use Lorentzian function then the overall shape of the correlation would be Lorentzian.

Which in our particular case of $x_0 = -20, k_0 = 3$ and $\delta = 1$ is the following

$$|C(\omega)|^2 = \frac{\frac{1}{2}e^{-4(9+20\sqrt{-2\omega+2\omega})} \left(1 + e^{(80-24i)\sqrt{-2\omega}} + e^{(80+24i)\sqrt{-2\omega}} + e^{160\sqrt{2\omega}}\right) (\omega + |\omega|)}{|\omega|^2\sqrt{\omega^2}} \quad (5.2)$$

The production of equation (5.2)¹⁶ with the transmission function (2.27) of the square well gives us the same result as our integrated projection of the WDF upon the frequency axes. Figure 26 shows a comparison of the results of the WDF integrated projection upon the frequency axis and the product of the transmission function with equation (5.2)

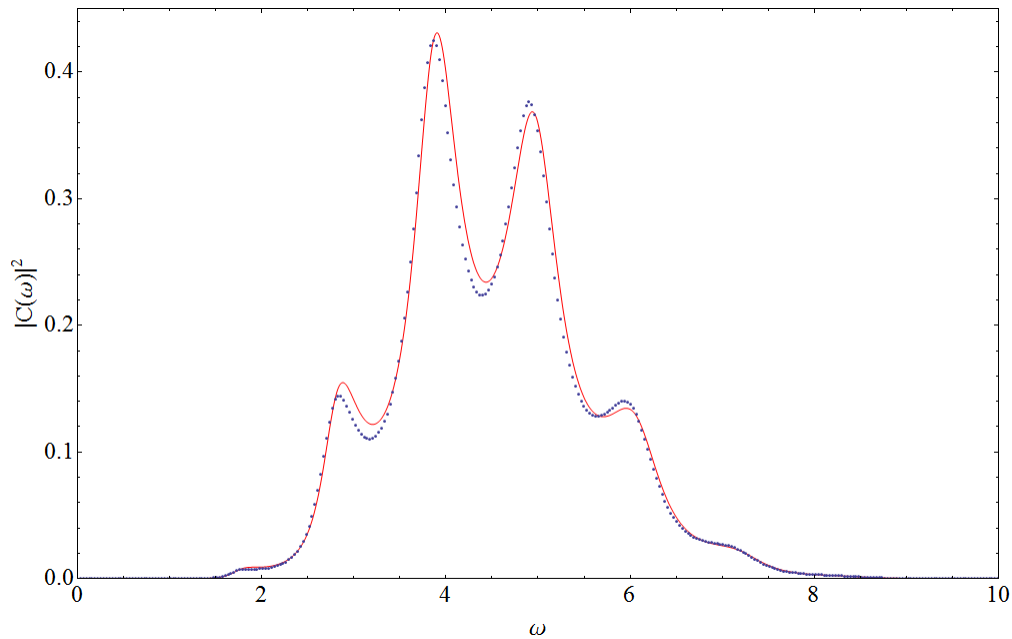


Figure 26. The comparison of the product of the transmission function (2.27) and equation (5.2) and the result of the integrated projection of the WDF upon the frequency axis. The red line is the product result and the blue dots are the results of the integration.¹⁷

¹⁶ This result was obtained by taking the Fourier Transform of $C(t)$ for the case where there was no potential well involved and finding the modulus of the result in Mathematica 6.0.

¹⁷ The slight differences in the red line and the blue dotted line potential arise from the discrete nature of the potential well and the fact that as mentioned in Section 4.2 the well is actually trapezoidal. It is the opinion of the author however that the difference has more to do with the analytical approximation Mathematica 6.0 made to reach the result in equation (5.2).

The integrated projection in time of a WDF generated from the time correlation of a wave function scattering off a potential well is the product of the transmission function of that potential well and the modulus of the frequency correlation of the wave function in free space. This property can be expanded to wells of unknown transmission functions and from it we can derive the transmission functions of those wells. By this we mean that we can take the correlation function of a scatter event off of those wells, generate a Wigner Distribution of that scattering, and integrate that distribution in time to get a probability density in terms of frequency. From here we can divide the probability density function by the modulus of the correlation function in frequency of a non-scattering event and from that arrive at our transmission function, which is what we should expect.

5.2. Square Well Energy Levels

Previously we saw that the integrated projection of the WDF corresponded to the transmission function of the square well we took our time correlation from. It is no surprise then to see that the resonant frequency levels match with the peak values of the WDF's integrated projection in frequency. However, if we take these frequency lines and place them across our 3 dimensional WDF surface, we see that the resonant frequency levels connect the positive peaks of every ridge structure in our surface. This is shown in figure 27.

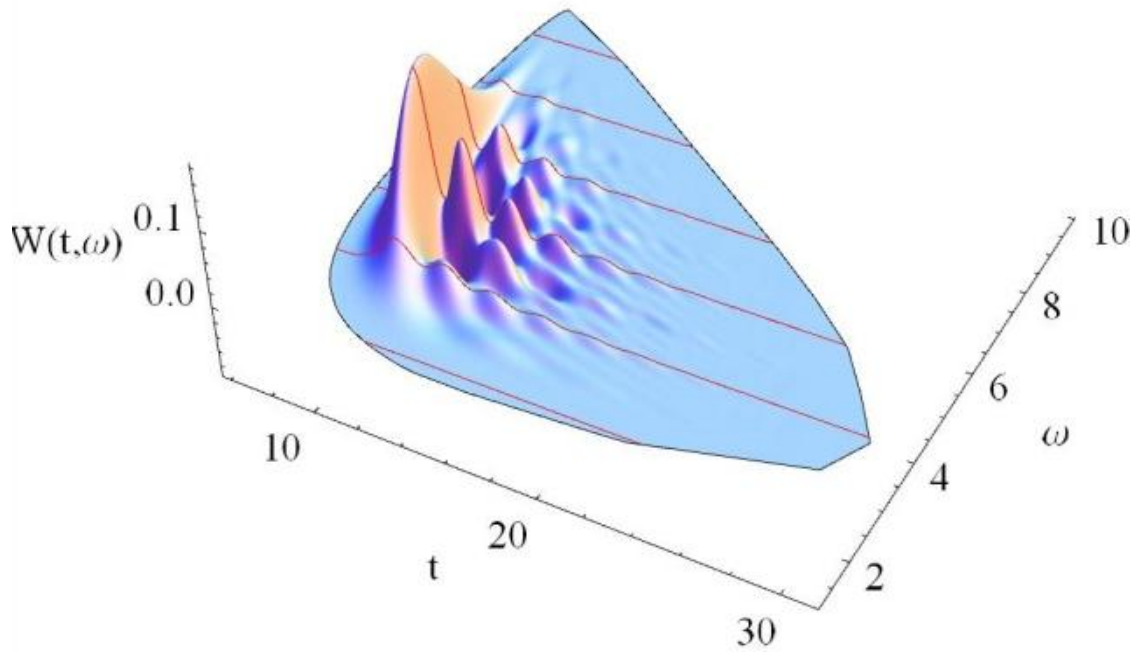


Figure 27. WDF plot with total transmission energy level bands of a well width of $40E_h$. The red lines indicate allowed frequencies for a quantum square well of depth $40E_h$ and width of $20a_0$.

However, that is not to say that these lines correspond to every positive peak position. If we examine the peak values of the third ridge structure in figure 27, by third ridge we mean the third positive structure seen as you progress along the time axis, we see that the frequency levels correspond to every other peak structure in that ridge line. There appears to be peaks that correspond to half way frequencies of the resonant frequencies. When the frequency levels of a well with double the actual scattered wells width are overlaid on top of the WDF surface we see that all the peaks in the third ridge line correspond to the new resonant frequencies, but we also notice that the preceding

ridge line, or second as you progress along the time axis, contains negative valley position along these lines “half” frequencies. This is shown in figure 28.

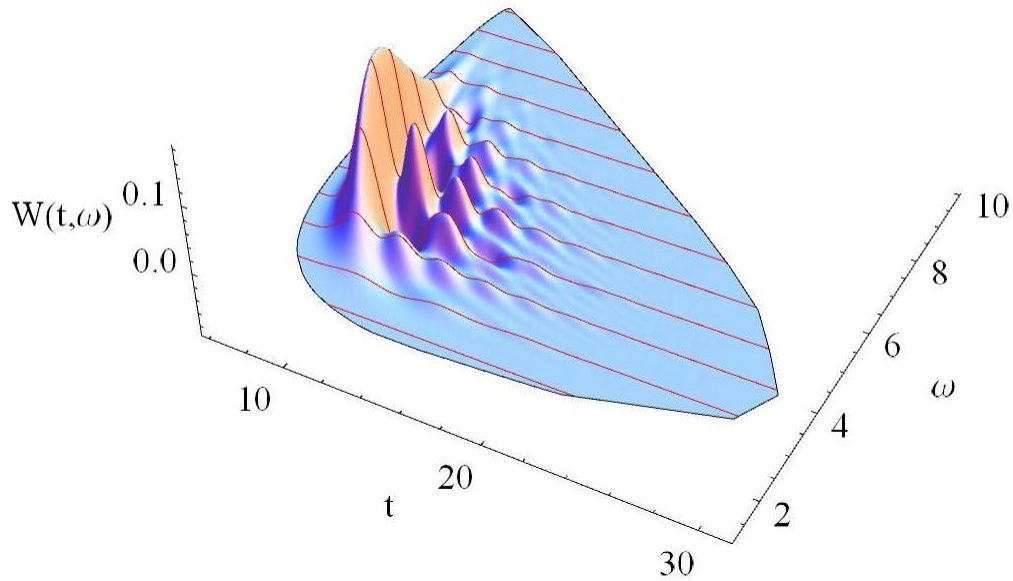


Figure 28. WDF plot with total transmission energy level bands of a well width of $40E_h$. The red lines indicate allowed frequencies for a quantum square well of depth $40E_h$ and width of $40a_0$.

Clearly the summation of these “half” frequencies is what leads to the positions of anti-resonant in the WDF’s integrate projection in frequency, but the meaning behind these negative values and corresponding positive features is unclear.

5.3. Time Arrivals

Yet another interesting feature we can observe in the WDF plot is the time arrival of a classical particle with an energy defined by $\hbar\omega$ in comparison with what we are seeing in the WDF plot. In the case of a classical particle with initial position equal to

the initial position of the wave function and energy equal to $\hbar\omega$, we can determine its arrival to the left edge of the square well by the following expression

$$t = \frac{x}{v} \quad (5.3)$$

Where $x = b$ and v are defined by the following,

$$E_{I,III} = \hbar\omega = \frac{1}{2}mv^2 \quad (5.4)$$

$$v_{I,III} = \sqrt{\frac{2\hbar\omega}{m}} \quad (5.5)$$

Since the time it would take to travel to and travel from the well is the same, we have denoted equations (5.4) and (5.5) for both region I, the region before the well, and region III, the region after the well. Once the particle enters the well, we assume it moves from the left edge to the right at a velocity described by the following expressions

$$E_{II} = \hbar\omega = \frac{1}{2}mv^2 - V_0 \quad (5.6)$$

$$v_{II} = \sqrt{\frac{2(\hbar\omega + V_0)}{m}} \quad (5.7)$$

Within the well the particle can do many different things. It can pass through the well. It can bounce off the right edge of the well and exit the well through the left edge. It can bounce off the right edge and then bounce off the left edge and exit the well back through the right edge. As you can see, the particle has an integer, n , number of scenarios of travel within the well before it finally exits. These scenarios can be expressed by multiplying the width of the well by the number of time the particle traverses the well

before exiting, n . A summation of all these expressions is given in equation (5.8) where the total time it takes the particle to reach the position of the stationary wave function is determined.

$$t(\omega) = \frac{2b}{\sqrt{\frac{2\hbar\omega}{m}}} + n \frac{2a}{\sqrt{\frac{2(\hbar\omega + V_0)}{m}}} \quad (5.8)$$

If we plot equation (5.8) for each positive integer value of n and set the resulting lines over top of our WDF plots, as done in figure 29, we can see that the overall ridge structure seen in the WDF plots correspond to this classical analogy.

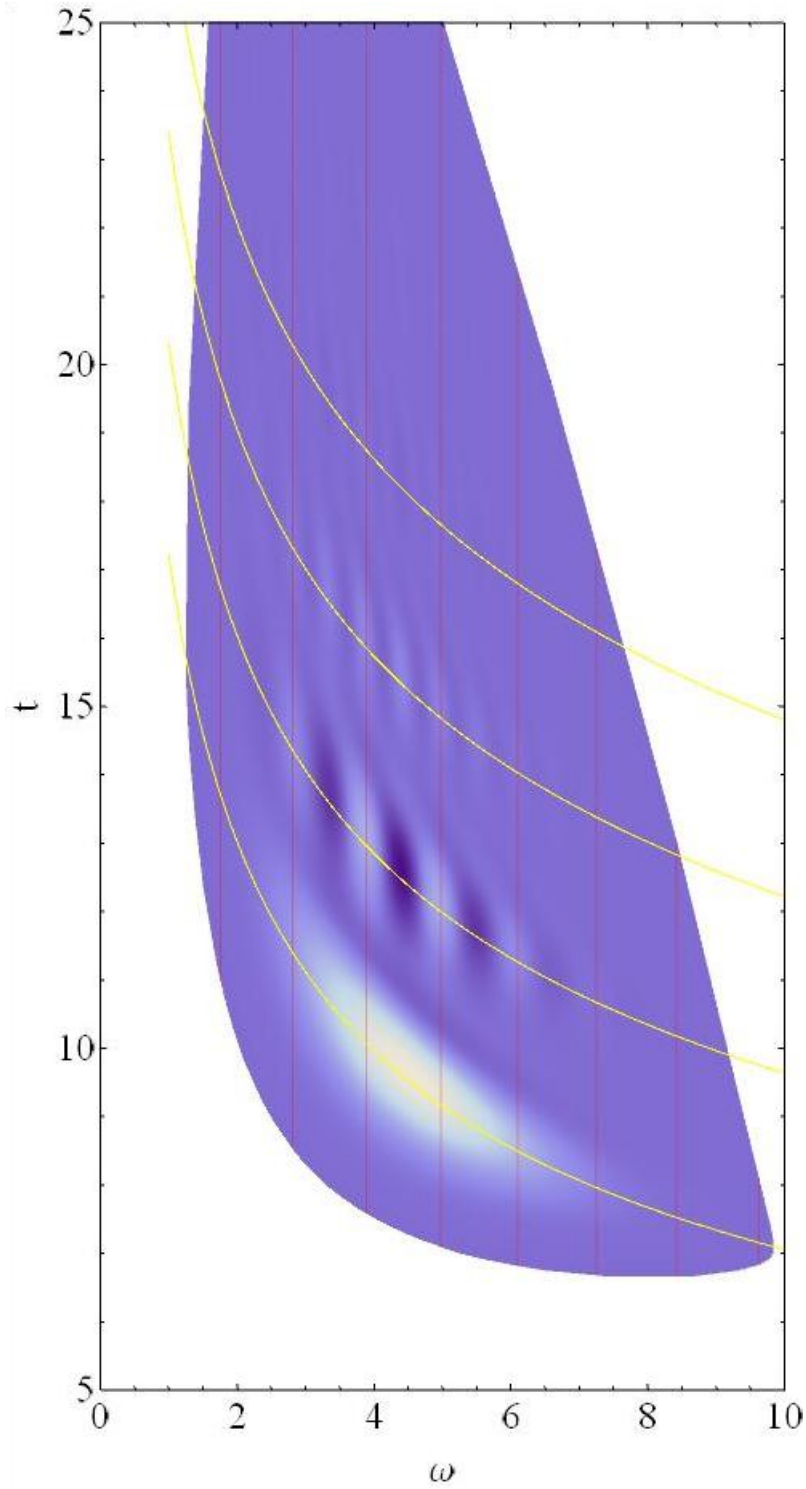


Figure 29. A contour plot of the WDF with yellow lines indicating the arrival times of a classical particle with the given frequency/energy while the red line indicate allowed frequencies of the quantum well.

While the first line represents the case where the classical particle proceeded directly through the square well, the second line represents the case where the particle bounced once off of the right wall of the well and exited the left side of the well, which is the side the particle entered the well initially. It is surprising to see that it is this classical example which corresponds to the ridge line where the positive peak values only occur at the energy levels of a square well of this type, (i.e. $a = 10$ and $V_0 = 20$). Classically, that information is leaving the well in left direction, but quantum mechanically that information is being recorded in the right region of the well.

5.4. Spectrogram versus WDF

Often in signal processing, the technique of taking a spectrogram is used in order to gauge contributions of frequency components within a signal. This is predominately used to weed out ambient noise and bolster desired frequencies. A spectrogram is the product of squaring a Short Time Fourier Transform, depicted in equation (5.9)

$$\chi(\tau, \omega) = \int s(t)w(t - \tau)e^{-i\omega t} dt \quad (5.9)$$

$$Spectrogram = |\chi(\tau, \omega)|^2 \quad (5.10)$$

The windowing function, $w(t - \tau)$, can be a multitude of functions from a Hanning function, a step function, to a Gaussian.

We applied this windowed Fourier Transform to our correlation function, as shown in figure 30, in order to see what information it provided of the scattering event in comparison to what we have gained from our WDF plots.

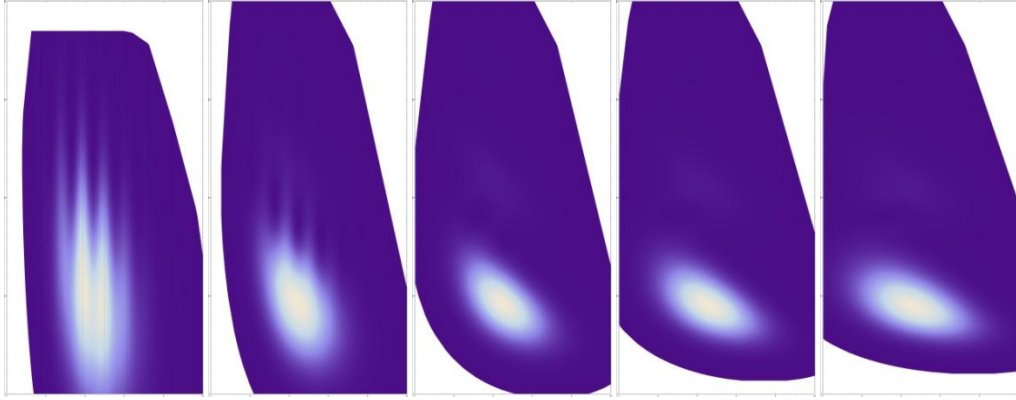


Figure 30. The windowed FT of our correlation function utilizing various FWHM values for the Gaussian window term. From right to left the value of c in equation (5.11) is as follows; 4.24661, 2.1233, 1.06165, 0.707768, and 0.530826 respectively.

We used a Gaussian for our windowing function

$$w(t - \tau) = e^{-\frac{(t-\tau)^2}{2\Delta t^2}} \quad (5.11)$$

From a cursory observation of the plots shown in figure 30 we see that most of the information returned in the spectrogram is obscured by the sheer volume of energy recorded in the initial large bulge of the correlation function. However, by applying a logarithmic scale to the spectrogram we were able to bring detailed elements of the scattering event back up to a scale where we could compare them with our WDF. Figure 31 shows these revised plots of the spectrograms.

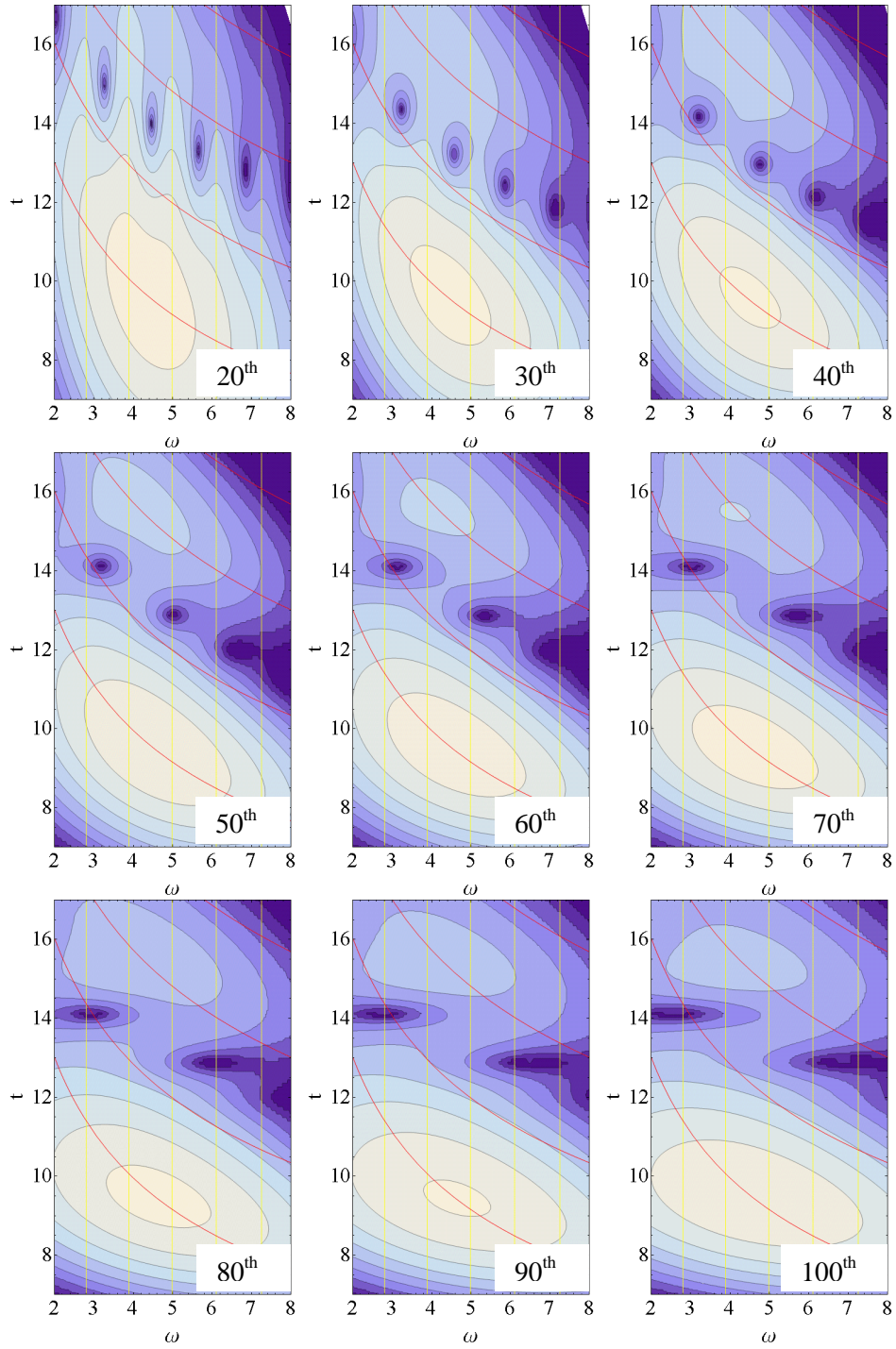


Figure 31. A series of spectrogram plots of a correlation function of the scattering event involving a well of depth $40E_h$ and width of $20a_0$. The box indicates the size in comparison to the overall time domain that the Gaussian window function, equation (5.11), set to when the spectrogram was generated. A N^{th} window size corresponds to a Δt given by the overall time of the correlation function divided by N , $\Delta t_N = 99.99/N$.

As shown in figure 31, a series of spectrograms were taken for the case of a correlation function generated from the scattering through a quantum potential square well of depth $40E_h$ and width of $20\alpha_0$. Each new spectrogram had the window size of the gaussian window function, equation (5.11), reduced in relation to the overall time of the correlation function. Since the length of time of the correlation function was 99.99(atomic time units) the gaussian window function was set to first be a 20th of that size, 4.9995(atomic time units), then a 30th, 3.333(atomic time units), and so on until a window size that was a 100th the time scale, .999 atomic time units. As was done with the WDF plots, the allowed frequencies and time arrival information was enterposed over top the contour plots of the spectrograms.

As you can see the allowed frequency information can be determined in spectrograms where a wide window was taken, 20th through about 40th. However, as the windowing function is narrowed, or we gain a greater degree of clarity in time, we loose our information in frequency. In figure 31, the 40th window spectrogram starts to show that the null regions, the small blue circles, between the allowed frequency bands begin to drift away from the center of those frequency bands until, as seen in the 50th window spectrogram, the null is located in regions of allowed frequency and in the 60th window spectrogram the null has moved into another spacing between energy bands.

On the converse as we loose this clarity frequency in smaller windowed spectrograms we tend to gain, to a small extent, clarity in time. All the spectrograms have the same general sweep as our time arrival lines, but it is not until you reach the 40th window spectrogram and then again in the 50th window spectrogram where you see the shape and place meant of these lines in nearest agreement. However, this is precisely the window scales that positioned out null, anti-resonance, at a position of resonance.

The spectrogram is a helpful tool in signal processing since the spectrogram is always a positive-valued distribution of energy in the signal. However the spectrogram comes at a cost that requires you to make a tradeoff in the precision of your time or frequency information. If we compare the outcomes of the spectrogram with our WDF shown in figure 29 we find that the WDF enumerates the same information (as shown in Section 5.2 and Section 5.3), but requires no trade-off be made in the time or frequency¹⁸.

5.5. Conclusion

The application of a correlation function to a scattering event and the production of its WDF have yielded a wealth of information about the long term effects a potential well has on a wave function. By analyzing the WDF plots of scattering events we have seen that it is possible to locate the allowed frequencies of the potential well. Additionally, the WDF tells us something, if only in terms of a classical kinematic analogy, of the time arrival of information of the reactant wave function after it has passed through the well.

Furthermore, the process of taking WDF plots of the correlation function of a scattered reactant wave function gives us a set of tools to analyze the reaction of quantum bodies with almost any potential well. Some of these tools include the reconstruction of the particular potential well's transmission function as well as the time departure beyond the potential frequencies. While the negative attributes of the WDF remain unintuitive to analysis, the WDF provides more insight into the potential scattering event than is gained from a Spectrogram of the same event. In the cases demonstrated here, the WDF can be

¹⁸ Although the ability for the WDF to hold negative values encourages us to avoid looking at it as an energy distribution as we were able to in the spectrogram, it is clearly analogous in most respects.

used in place of a spectrogram to return the same information the spectrogram could provide without the need for scaling window size. It is in the opinion of the author that applications of WDF plots in broader chemical reactions will provide researchers in the field of chemical physics a broader interpretation of the reaction as a whole.

5.6. Further Research

Recommendations of further work would be to generate correlation functions of the exiting propagating wave function from both sides of the potential well and compare their WDF plots. As well as comparing the WDF plots to other signals processing techniques such as the ambiguity function (see Appendix B). Additionally, expanding the application of generating WDF from correlation functions of 2 and 3 dimensions potential scattering events as well as coupled potential wells.

Appendix A

The WDF produced by scattering our propagating wave through a series of Gaussian and triangular potential well showed remarkably little results. Since the FORTRAN code was designed to have the potential well occupy the region of $x = -10$ to $x = 10$ it is possible that as we increased the depth of the potential well, the overall shape of our Gaussian function and triangular functions became closer approximations of a delta function then occurred in the square or circular case. In the case of a delta function there is no internal well width for the wave to bounce within and the propagation become analogous to the free particle example with no well to scatter upon. When the wells are shallower then it is also possible that the β term is not large enough for resonant feature to become prominent over the initial transfer of frequency as the wave pass through the wall once.

Additionally, it is possible that the angle of the well barrier is what cased this lack of feature. In the Square and Circular well the angle made between the region of space with no well and the region of space with a well is 90° . In the case of the Gaussian and Triangular Wells that angle is either gradual or less than 90° . This is depicted in figure 31.

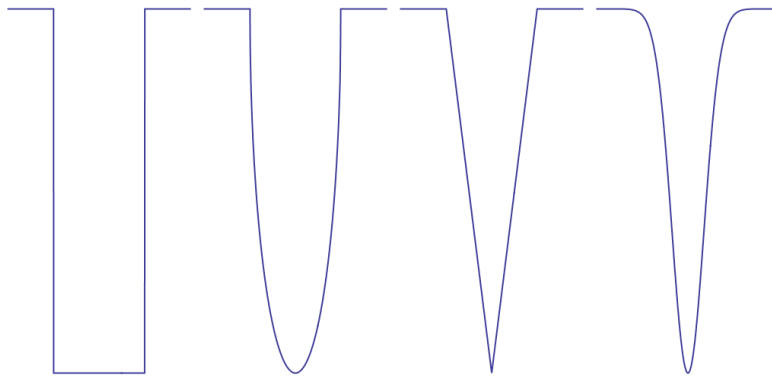


Figure 32. The well shapes used as the potential component of the Spilt Operator Method. From right to left they are a square well, a circular well, a triangular well, and a Gaussian well.

Gaussian Well

Provided below are the WDF plot generated for a potential well given by equation (A.1) where V_0 is the depth of the well.

$$V(x) = -V_0 e^{-x^2} \quad (\text{A.1})$$

Gaussian $V_0 = 10 E_h$

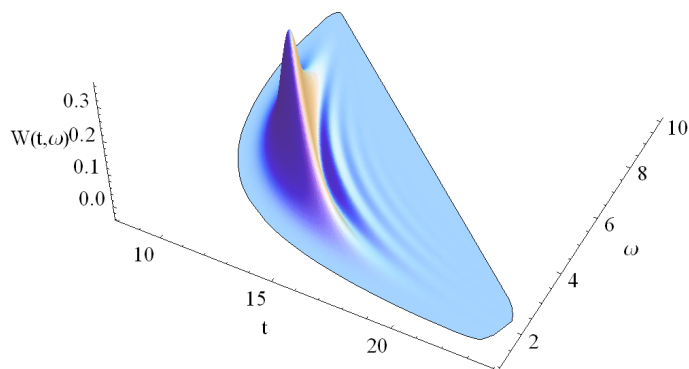


Figure 33. Depiction of a WDF plot generated from the time correlation function of a reactant wave function scattering through a quantum Gaussian well of $10E_h$.

Gaussian $V_0 = 20 E_h$

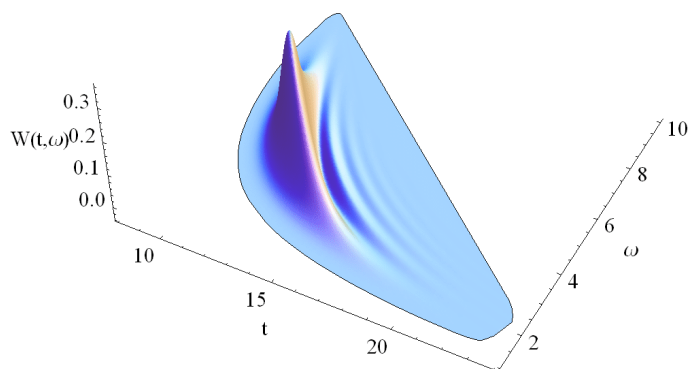


Figure 34. Depiction of a WDF plot generated from the time correlation function of a reactant wave function scattering through a quantum Gaussian well of $20E_h$.

Gaussian $V_o = 40 E_h$

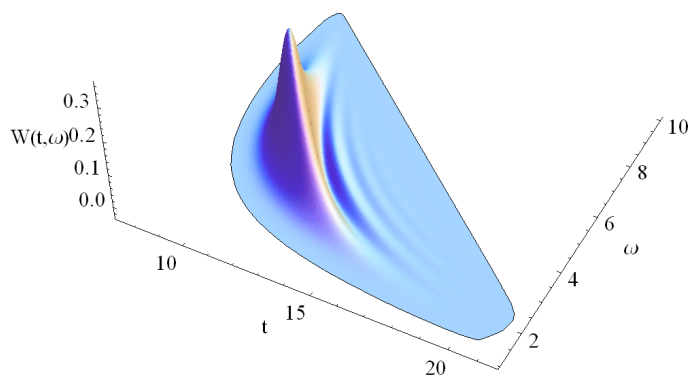


Figure 35. Depiction of a WDF plot generated from the time correlation function of a reactant wave function scattering through a quantum Gaussian well of $40E_h$.

Gaussian $V_o = 60 E_h$

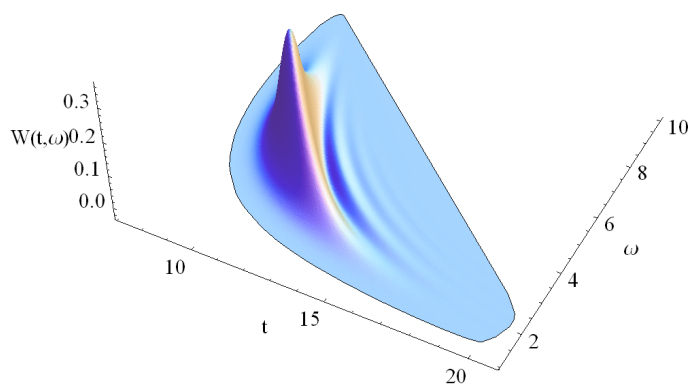


Figure 36. Depiction of a WDF plot generated from the time correlation function of a reactant wave function scattering through a quantum Gaussian well of $60E_h$.

Gaussian $V_0 = 80 E_h$

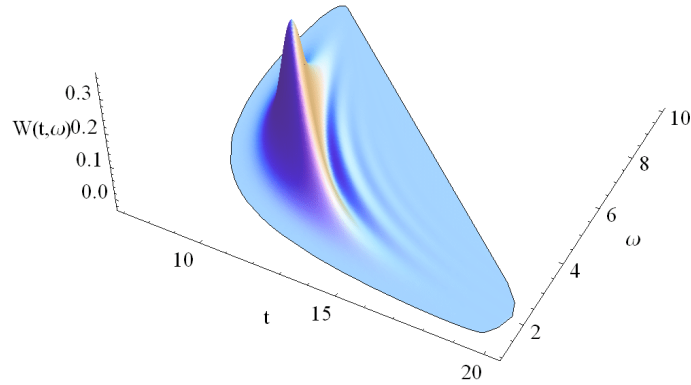


Figure 37. Depiction of a WDF plot generated from the time correlation function of a reactant wave function scattering through a quantum Gaussian well of $80E_h$.

Triangular Well

Provided below are the WDF plot generated for a potential well given by equation (A.2) where V_0 is the depth of the well and a is the width of the well at the base of the triangle.

$$V(x) = \begin{cases} -V_0 + \frac{V_0}{a}|x| & -a < x < a \\ 0, & |x| > a \end{cases} \quad (\text{A.2})$$

Triangular $V_o = 10 E_h$

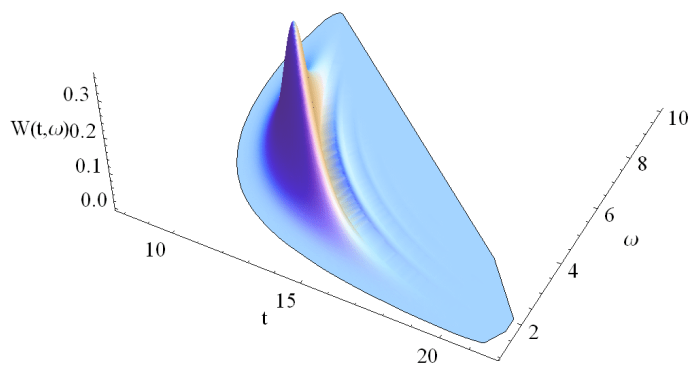


Figure 38. Depiction of a WDF plot generated from the time correlation function of a reactant wave function scattering through a quantum triangular well of $10E_h$.

Triangular $V_o = 20 E_h$

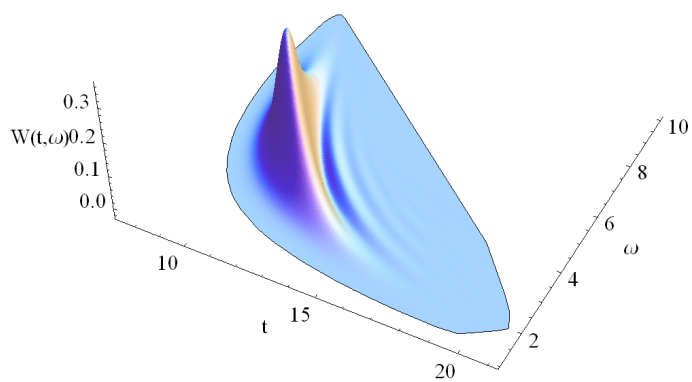


Figure 39. Depiction of a WDF plot generated from the time correlation function of a reactant wave function scattering through a quantum triangular well of $20E_h$.

Appendix B

In addition to rescaling the spectrogram data by use of taking the logarithmic value at each point in the time frequency domain we also normalized those same values versus the entirety of the spectrogram. By taking this approach we were able to bring up smaller features that were obscured by the size of the primary peaks in the spectrogram. Below (Figure 40 and 41) is the results of these normalized spectrogram displayed in a similar manner to the plots shown in figure 31.

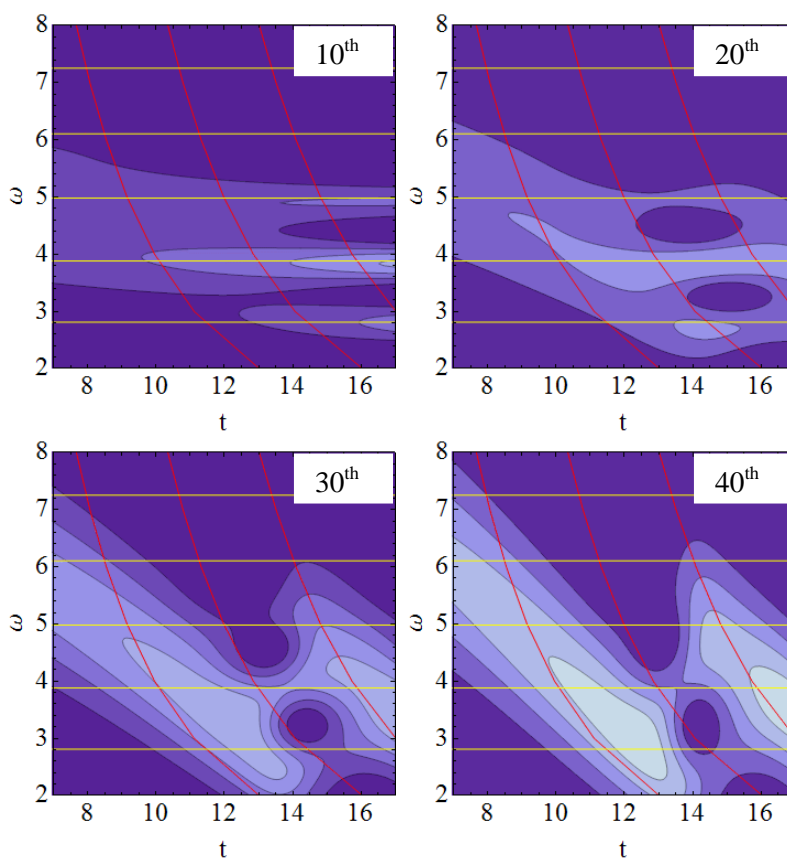


Figure 40. Normalized spectrograms of the generated correlation function of the scattering event involving a well of depth $40E_h$ and width of $20a_0$. The red lines indicate the classical time arrival of a particle with energy given by ω and the yellow lines represent the allowed transmission resonances of the square well. Window sizes of a 10th, 20th, 30th and 40th of the overall time length of the correlation are given shown.

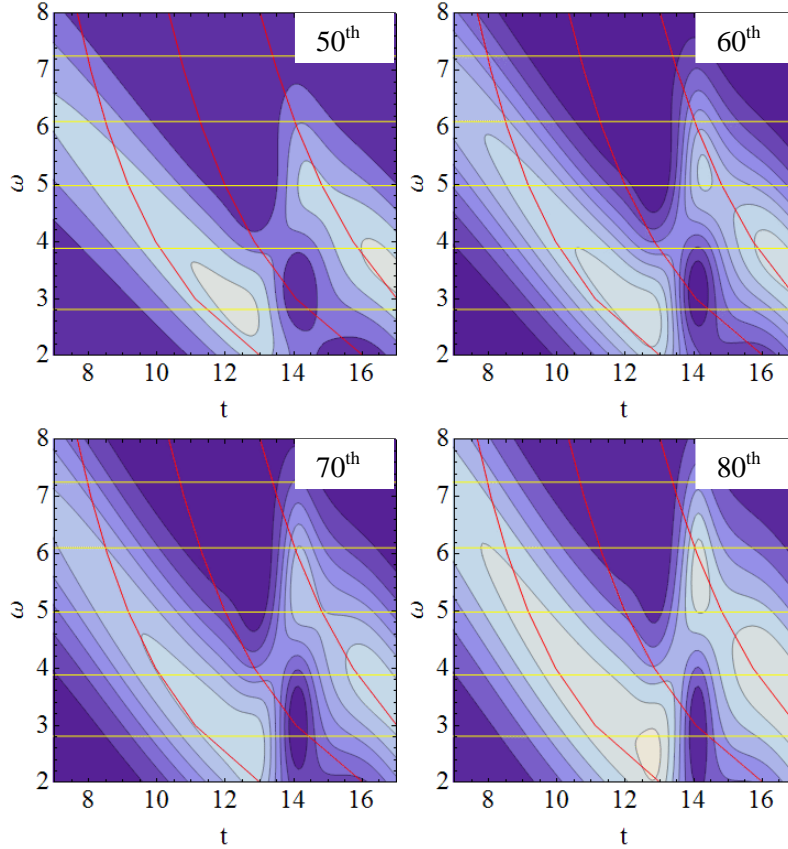


Figure 41. Normalized spectrograms of the generated correlation function of the scattering event involving a well of depth $40E_h$ and width of $20a_0$. The red lines indicate the classical time arrival of a particle with energy given by ω and the yellow lines represent the allowed transmission resonances of the square well. Window sizes of a 50th, 60th, 70th and 80th of the overall time length of the correlation are given shown.

We observed that once the normalized spectrogram was taken it was far easier to draw a comparison between the classical time arrival analysis and the information seen in the spectrogram. However, the tradeoff between the accuracy of the frequency component to the time component of the spectrogram is still present as well saw in the logarithmic version. As we refine our windowing function in time we can see that the null regions between our transmission resonance lines move out of the regions between the resonance lines and spread to overlap regions of transmission. As discussed previously, this time/frequency trade-off is absent in the Wigner Distribution Function.

Appendix C

Another function used in signal processing is the Ambiguity function as shown in equation (B.1). [19]

$$\chi(\tau, \omega) = \int s(t + \tau)s^*(t - \tau)e^{-i\xi t} dt \quad (\text{C.1})$$

This function is typically used in the radar community to observe the Doppler delay of a radar pulse upon a moving target. Figure 40 depicts the real and imaginary components of the Ambiguity function for a complex Gaussian centered about $x = 2.5$ and all other attributes set to unity. Figure 41 depicts the modulus of the ambiguity function of the same Gaussian already described.

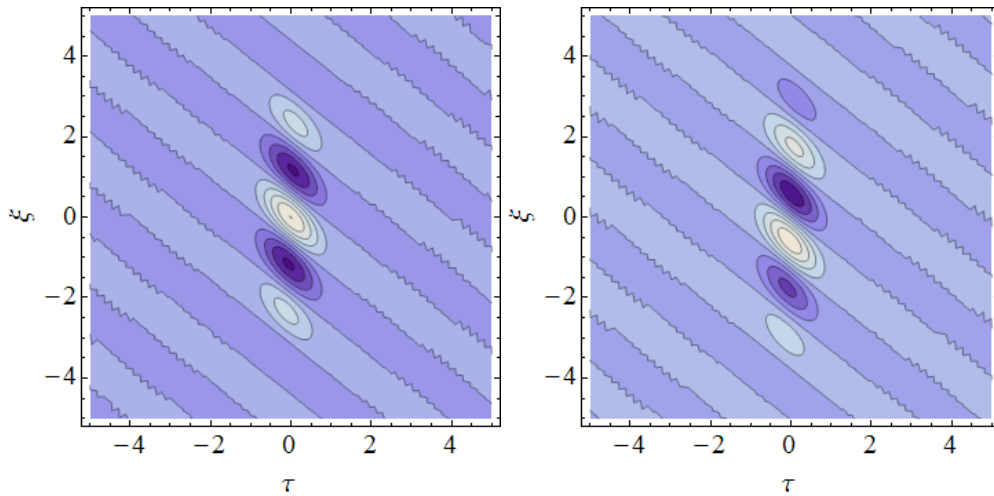


Figure 42. Ambiguity function (real component on the left and imaginary component on the right) of a complex Gaussian centered about $x = 2.5$ and all other attributes set to unity.

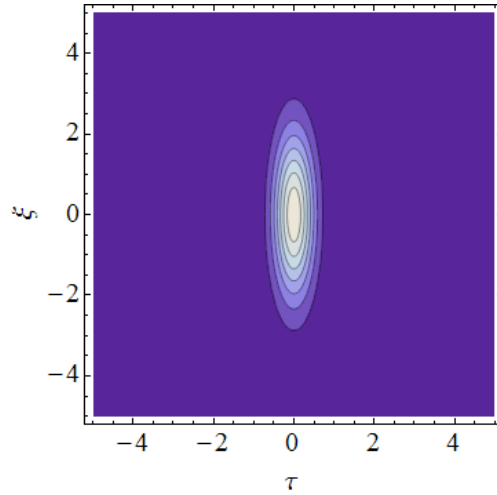


Figure 43. The modulus of a Ambiguity function of a complex Gaussian centered about $x = 2.5$ and all other attributes set to unity.

This function could also be used to analyze the correlation function generated in our methods described in Section II. An example of such an ambiguity function is shown in figure 42 for the case of a correlation function generated from scattering through a quantum potential square well of depth $40E_h$ and width of $20\alpha_0$.

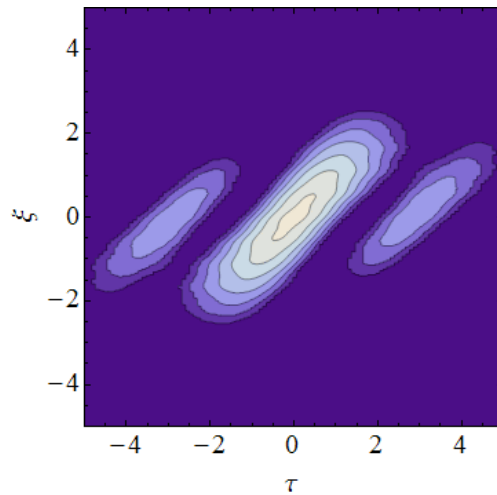


Figure 44. The modulus of an Ambiguity Function of a correlation function generated from scattering through a quantum potential square well of depth $40E_h$ and width of $20\alpha_0$. Represented on a logarithmic scale.

Bibliography

- [1] T. A. C. M. Claasen and W. F. G. Mecklenbräuker, "The Wigner Distribution - A Tool For Time-Frequency Signal Analysis Part I: Continuous-Time Signals," *Philips Journal of Research*, vol. 35, no. 3, pp. 217-250, 1980.
- [2] E. P. Wigner, "On the quantum correlation for thermodynamic equilibrium," *Physics Review*, vol. 40, pp. 749-759, 1932.
- [3] G. B. Arfken and H. J. Weber, *Mathematical Methods for Physicists*, Sixth Edition ed. Burlington, Maryland: Elsevier Inc., 2005.
- [4] J. D. Gaskill, *Linear Systems, Fourier Transforms, and Optics*. New York, New York: John Wiley & Sons, 1978.
- [5] D. J. Griffiths, *Introduction to Quantum Mechanics*. Upper Saddle River, New Jersey: Prentice Hall, Inc., 1995.
- [6] R. L. Liboff, *Introductory Quantum Mechanics*, Fourth Edition ed. San Francisco, California: Pearson Education, Inc., 2003.
- [7] E. Merzbacher, *Quantum Mechanics*, 2nd ed. New York: John Wiley & Sons, Inc., 1970.
- [8] D. E. Weeks and D. J. Tannor, "A time-dependent formulation of the scattering matrix using Møller operators," *Chemical Physics Letters*, no. 307, pp. 301-308, 1993.
- [9] D. E. Weeks and R. S. Calfas, "Air Force Technical Report".
- [10] T. A. Niday, Thesis AFIT/GAP/ENP/99M-06, Wright-Patterson AFB OH, 1999.
- [11] D. V. Vlasov, "Optimization of the Split-Operator Method for Modeling of Quantum System Time Evolution," vol. IV, no. 2, 2005.
- [12] D. J. Griffiths, *Introduction to Quantum Mechanics*. Upper Saddle River: Prentice Hill, Inc., 1995.
- [13] C. Cohen-Tannoudji, B. Diu, and F. Lulöe, *Quantum Mechanics*. vol. I.
- [14] D. J. Tannor and D. E. Weeks, "Wave packet correlation function formulation of scattering theory: The quantum analog of classical S-matrix theory," *The Journal of Chemical Physics*, no. 98, pp. 3884-3893, 1993.

- [15] H. Shull and G. G. Hall, "Atomic Units," *Nature*, vol. 184, no. 4698, p. 1559, 1959.
- [16] R. L. Burden and J. D. Faires, *Numerical Analysis*, 8th ed. Belmont, CA: Thomson Brooks/Cole, 2005.
- [17] J. W. Goodman, *Introduction to Fourier Optics*, 3rd ed. Greenwood Village: Roberts & Company Publishers, 2005.
- [18] R. S. Calfas and D. E. Weeks, "A new application of absorbing boundary condition for computing collinear quantum reactive scattering matrix elements," *Chemical Physics Letters*, no. 263, pp. 292-296, 1996.
- [19] T. A. C. M. Claasen and W. F. G. Mecklenbräuker, "The Wigner Distribution - A Tool for Time Frequency Signal Analysis Part III: Relations with other Time-Frequency Signal Transformations," *Philips Journal of Research*, vol. 35, no. 6, pp. 372-389, 1980.
- [20] J. E. Moyal, "Quantum mechanics as a statistical theory," *Proceeding of the Cambridge Philosophical Society*, no. 45, pp. 99-124, 1949.
- [21] P. A. Dirac, "Note on exchange phenomena in the Thomas atom," *Proc. Camb. Phil. Soc.*, no. 26, pp. 376-395, 1930.

Vita

Captain Brent Lacy has spent much of his life in the United States Air Force. Born on Ellsworth AFB he spent most of his life until High School moving with his family in pursuit of his father's Military career. He attended the University of Texas in Austin from 1999 to 2003 and received a Bachelor of Science Degree in Physics. During that time he served in the Air Force Reserve Officer Training Course, Detachment 825, on campus. Upon graduation he was commissioned in the Air Force as a Second Lieutenant. His first assignment took him to Fort George G. Meade in Maryland and during that tour he met his wife. At the time of this publication he was completing his assignment to AFIT where he earned a degree in Applied Physics.

REPORT DOCUMENTATION PAGE				Form Approved OMB No. 074-0188	
The public reporting burden for this collection of information is estimated to average 1 hour per response, including the time for reviewing instructions, searching existing data sources, gathering and maintaining the data needed, and completing and reviewing the collection of information. Send comments regarding this burden estimate or any other aspect of the collection of information, including suggestions for reducing this burden to Department of Defense, Washington Headquarters Services, Directorate for Information Operations and Reports (0704-0188), 1215 Jefferson Davis Highway, Suite 1204, Arlington, VA 22202-4302. Respondents should be aware that notwithstanding any other provision of law, no person shall be subject to a penalty for failing to comply with a collection of information if it does not display a currently valid OMB control number. PLEASE DO NOT RETURN YOUR FORM TO THE ABOVE ADDRESS.					
1. REPORT DATE (DD-MM-YYYY) 26-03-2009		2. REPORT TYPE Master's Thesis		3. DATES COVERED (From - To) Jun 2008 - Mar 2009	
4. TITLE AND SUBTITLE A Wigner Distribution Analysis of One Dimensional Scattering				5a. CONTRACT NUMBER	
				5b. GRANT NUMBER	
				5c. PROGRAM ELEMENT NUMBER	
6. AUTHOR(S) Lacy, Brent R., Captain, USAF				5d. PROJECT NUMBER	
				5e. TASK NUMBER	
				5f. WORK UNIT NUMBER	
7. PERFORMING ORGANIZATION NAMES(S) AND ADDRESS(S) Air Force Institute of Technology Graduate School of Engineering and Management (AFIT/EN) 2950 Hobson Way, Building 640 WPAFB OH 45433-8865				8. PERFORMING ORGANIZATION REPORT NUMBER AFIT/GAP/ENP/09-M06	
9. SPONSORING/MONITORING AGENCY NAME(S) AND ADDRESS(ES) AFSOR (AFMC) ATTN: Dr. Michael R. Berman 875 North Randolph Street, Suite 325, Room 3112 Arlington, Va., 22203-1768 DSN: 426-7781				10. SPONSOR/MONITOR'S ACRONYM(S)	
				11. SPONSOR/MONITOR'S REPORT NUMBER(S)	
12. DISTRIBUTION/AVAILABILITY STATEMENT APPROVED FOR PUBLIC RELEASE; DISTRIBUTION UNLIMITED.					
13. SUPPLEMENTARY NOTES					
14. ABSTRACT We applied the Wigner Distribution Function, a distribution function of time and frequency based on an initial function of either of those variables, to a series of time based correlation functions. These time based correlation functions were the result of a 1-dimensional free particle wave packet, the reactant wave function, which had propagated through a quantum potential well and then had components of the reactant wave function that exited the opposite side of the well auto-correlated in time with a stationary 1-dimensional free particle wave packet, the product wave function. This process was undertaken in order to generate a 3-dimensional depiction, in time and frequency, of the reactant wave functions interaction with the quantum potential well. Fortran 77 code was utilized to generate the time propagation of the reactant wave function by means of the Split Operator Method, which was given the following initial set of conditions; $x_0 = -20$ (Bohr radii), $k_0 = 3$ (atomic units), and $\delta = 1$ (Bohr radius). A series of potential wells with variable depths were implemented into the code. The code then computed the correlation in time of the exiting reactant wave function with a stationary wave function before applying the Wigner Distribution Function. When Wigner Distribution Function was applied to the time correlation function many recognizable features on the potential well were observed from the 3-deminsional plot generated including transmission resonance energy levels. The classical time of arrival was also captured by the Wigner Distribution Function. As a useful tool the Wigner Distribution Function provides more insight into the quantum interactions of chemical reactions in terms of time and frequency than traditional spectrographic analysis.					
15. SUBJECT TERMS Spilt Operator Method, Correlation Function, Reactant Wave Packet, Product Wave Packet, Wigner Distribution Function, Ambiguity Function, Short Time Fourier Transform, Spectrogram, Aliasing, Scattering Theory, Quantum Potential Well, Quantum Square Well					
16. SECURITY CLASSIFICATION OF:			17. LIMITATION OF ABSTRACT UU	18. NUMBER OF PAGES 87	19a. NAME OF RESPONSIBLE PERSON Dr. David E. Weeks (ENP)
a. REPORT U	b. ABSTRACT U	c. THIS PAGE U			19b. TELEPHONE NUMBER (Include area code) (937) 255-3636, ext. 4561 david.weeks@afit.edu

Standard Form 298 (Rev. 8-98)
Prescribed by ANSI Std. Z39-18